nks
Nordisk kernesikkerhedsforskning
Norrænar kjarnöryggisrannsóknir
Pohjoismainen ydinturvallisuustutkimus
Nordisk kjernesikkerhetsforskning
Nordisk kärnsäkerhetsforskning
Nordic nuclear safety research

NKS-231
ISBN 978-87-7893-302-7

Comparison of VNEM to Measured Data from Ringhals Unit 3 (Phase 3)

Makoto Tsuiki and Steven Mullet

Institute for Energy Technology, OECD Halden Project, Norway

January 2011

Abstract

1. PWR
Comparisons have been made of a PWR core simulator CYGNUS with VNEM neutronics module to the measured data obtained from Ringhals unit 3 NPP through the cycle 1A (core average burnup = 0 through 10,507MWD/MT).
The results can be summarized as:
core eigenvalue = 0.99937 +/- 0.00086 before intermediate
5 months shutdown
core eigenvalue = 0.99647 +/- 0.00029 after intermediate
5 months shutdown
The reason of core eigenvalue drop after the intermediate shutdown is estimated to be the build-up of fissile elements during the long shutdown. A calculation model to track some important isotopes in addition to Xe135 and Sm149 (these isotopes are tracked in the present version of CYGNUS) has to be implemented.
As for the comparison of the neutron detector readings, the agreement was excellent throughout the cycle 1A as observed in Phase 1 and 2 (2008, 2009).
The burnup tilt effect was not observed during the cycle 1A. The verification of the burnup tilt model of CYGNUS will be performed in the next phase of the project.

2. BWR
A preliminary 2D numerical benchmarking was performed for BWR cores. The problems were generated imitating the NEACRP MOX PWR 2D benchmark problems. The results of comparisons of VNEM to a reference transport code (FCM2D), based on the method of characteristics, were as good as those obtained in the case of PWR cores for similar benchmarking.

Key words

CYGNUS, VNEM, Ringhals, unit 3, PWR, neutron detector, keff, BWR, benchmark,
IACIP: NKS_R_2008_61

NKS-231
ISBN 978-87-7893-302-7

Electronic report, January 2011

NKS Secretariat
NKS-776
P.O. Box 49
DK - 4000 Roskilde, Denmark

Phone +45 4677 4045
Fax +45 4677 4046
www.nks.org
e-mail nks@nks.org

	Document type	Page
Institutt for energiteknikk **OECD HALDEN REACTOR PROJECT**	ANNUAL REPORT	1/44
Org./Author	Date Code	
IFE / Makoto Tsuiki and Steven Mullet	10.12.2010 AR-CYGNUS-NKS-01-10 (r0)	
Distribution	Checked by	Date
NKS-R Program Manager	IFE / Jan Porsmyr	
VTT	Approved by	Date
	IFE / Davide Roverso	
	Replaces	Retention time
		☐ <7 ☐ 8...14 ■ >15

Keywords
CYGNUS, VNEM, Ringhals, unit 3, PWR, neutron detector, keff, BWR, benchmark,
IACIP: NKS_R_2008_61

Comparison of VNEM to Measured Data from Ringhals Unit 3 (Phase 3)

Purpose

According to the agreement between NKS-R Program Management and Institutt for Energiteknikk (IFE), a verification study of the transport variational nodal expansion method (VNEM) has been performed based on the specification in the activity plan. This report presents the results of the study in detail.

Abstract

1. PWR

Comparisons have been made of a PWR core simulator CYGNUS with VNEM neutronics module to the measured data obtained from Ringhals unit 3 NPP through the cycle 1A (core average burnup = 0 through 10,507MWD/MT).

The results can be summarized as:

core eigenvalue = 0.99937 ± 0.00086 before intermediate 5 months shutdown
core eigenvalue = 0.99647 ± 0.00029 after intermediate 5 months shutdown

The reason of core eigenvalue drop after the intermediate shutdown is estimated to be the build-up of fissile elements during the long shutdown. A calculation model to track some important isotopes in addition to Xe135 and Sm149 (these isotopes are tracked in the present version of CYGNUS) has to be implemented.

As for the comparison of the neutron detector readings, the agreement was excellent throughout the cycle 1A as observed in Phase 1 and 2 (2008, 2009).

The burnup tilt effect was not observed during the cycle 1A. The verification of the burnup tilt model of CYGNUS will be performed in the next phase of the project.

2. BWR

A preliminary 2D numerical benchmarking was performed for BWR cores. The problems were generated imitating the NEACRP MOX PWR 2D benchmark problems. The results of comparisons of VNEM to a reference transport code (FCM2D), based on the method of characteristics, were as good as those obtained in the case of PWR cores for similar benchmarking.

Table of Contents

1 Introduction

This report shows the results of the comparisons of a light water reactor core simulator *CYGNUS* to the plant data obtained from Ringhals-3 pressurized water reactor (PWR) through the cycle 1A (01.10.1980 - 01.06.1983, exposure increment = 10,507MWD/MT).

In addition, a preliminary results of numerical benchmarking of VNEM in the case of BWR cores are shown.

In the year *2008* the verification of nodal transport code VNEM (Variational Nodal Expansion Method) was performed by comparing it to the plant data from Ringhals-3 PWR in a hot stand-by condition without feedback effects (the thermal-hydraulic, burnup, Xenon, Doppler, etc.) at the beginning of its life. The results of the comparisons were excellent as reported in Ref.[2.1].

In the year *2009* VNEM was implemented in a light water reactor core simulator CYGNUS (PWR version) to include the feedback effects. Comparisons of CYGNUS to plant data from Ringhals-3 have been made for hot-operating cases from the beginning of life of the core up to the average burnup of about 500MWD/T.

In the year *2010* we made the core follow calculation of whole cycle 1A of Ringhals-3 by CYGNUS, mainly expecting to verify the intra-nodal burnup tilt (the effect of the difference of intra-assembly spatial burnup distribution from the infinite-lattice case on the neutron cross sections) model. However, the tilt effect found to be insignificant even at the end of the cycle 1A. Instead we found a significant k_{eff} drop after long term shutdown. The reason of this drop is estimated to be the build-up of some fissile isotopes during the shutdown (the shut-down cooling effect). We are now developing a model to calculate the shut-down cooling effect and we wish to verify the model in the next phase of this project.

We also wish to continue the core follow calculation of Ringhals-3 for farther cycles to verify the intra-nodal burnup tilt model.

In Chapter 2 the results of the core follow calculation of Ringhals-3, cycle 1A are described in detail. In Chapter 3 the results of numerical benchmarking of BWR cores are discussed. Chapter 4 shows the conclusion and the future work.

2 Core Follow Calculation of Ringhals-3, Cycle 1A

2.1 Method

The codes used in this study are the same as in Reference [2.1], i.e., we use the followings:

- HELIOS[2.2] : lattice code
- VCOEF[2.1] : VNEM coeffecients generation code
- VTABLE[2.1] : VNEM coefficients tabulation code
- CYGNUS[2.1] : core simulator

The group neutron transport equations are solved based on the VNEM in the neutronics module of CYGNUS code, to obtain the group neutron flux and the power density distributions in the reactor core and the core eigenvalue (effective multiplication factor). The coefficients of the equations depend on the parameters listed at the beginning of Chapter 2 of Reference [2.1].

To include the effects of parameters (the burnup, Boron concentration, Xenon-135 concentration, etc.) on the VNEM coefficients, as in many of the existing systems, the whole calculation process is divided into 2 stages: the single-assembly, infinite-lattice calculation stage (Stage 1) and the global, full core calculation stage (Stage 2).

In Stage 1, by using a lattice burnup code HELIOS [2.2] and *VCOEF-VTABLE* codes[2.1], tables of the VNEM coefficients are parametrically generated.

Stage 2 is performed by CYGNUS code. In the coefficients reproduction module of CYGNUS the VNEM coefficients are reproduced node-by-node depending on the values of the feedback parameters of a node, by using the tables of the coefficients generated in Stage 1.

In the year 2010 we made the following improvements:

- Normalization of the infinite multiplication factor to the lattice code (HELIOS)
- Inclusion of the Sm-149 transient effect
- Inclusion of the instantaneous Boron effect

in generating the VNEM coefficients.

2.1.1 Normalization of Infinite Multiplication Factor to Lattice Code

In a 2-dimensional, infinite-lattice case, the infinite-multiplication factor (k^{∞}) obtained by VNEM should be equal to that obtained from the lattice code. However this is not guaranteed because the methods of solving the transport equation in the lattice code and VCOEF are different. For example, in HELIOS it is the collision probability method and in VCOEF, the method of characteristics. The number of energy groups are also different (generally the lattice code adopts fine energy group structure).

Therefore it is desirable that VCOEF reproduces the same k^{∞} as the lattice code, as generally the latter is doing more accurate calculations. This is performed by normalizing the fission neutron yielding cross section as:

$$\nu\Sigma^{f}_{g,\,\text{normalized}} = a.\nu\Sigma^{f}_{g,\,\text{unnormalized}} \qquad (2.1.1)$$

where the normalization factor a is obtained by

$$a = k^{\infty}_{\text{lattice code}} / k^{\infty}_{\text{VCOEF}} \quad (2.1.2)$$

and

$k^{\infty}_{\text{lattice code}} = k^{\infty}$ calculated by the lattice code
$k^{\infty}_{\text{VCOEF}} = k^{\infty}$ calculated by VCOEF code

2.1.2 Inclusion of Samarium-149 Transient Effect

In Reference [2.1], the concentration of Sm-149 was assumed to be zero, by setting the input parameter:

ISMRIUM = 0,

because the calculation was limited to the beginning of the life of the core. This is not the case in the work this year. So we assumed that the concentration of Sm-149 in a node is the same as that given by HELIOS code for the same burnup, by setting

ISMRIUM = 1.

By this setting of ISMRIUM, CYGNUS assumes that the transient behavior of Sm-149 is given by the base coefficients matrix[2.1], i.e., Sm-149 builds up depending on the burnup as in HELIOS.

2.1.3 Inclusion of Instantaneous Boron Effect

In reference [2.1], the historical Boron concentration was assumed to be equal to the instantaneous Boron concentration, because the core follow calculation was limited to near the beginning of the life of the core. This is not the case in the work this year, therefore we use both the instantaneous and the historical Borons separately as explained in Section 2.2 and 2.3 of Reference [2.1].

2.2 Results

Various points were selected for CYGNUS core calculations based on a number of factors. The core follow data file for cycle 1A given to IFE by Ringhals lists the core data a few times per day (sometimes it is listed hourly, but usually it is closer to 3 times per day). Each core follow point consists of the date, time, D-bank position, C-bank position, water temperature, core thermal power, CTP percent, burnup, and pressure. The pressure stays constant at 154 bar at all times. The boron level is also listed sporatically in the core follow data file (see Figure 5.1). Since the boron level is crucial to the calculation, points were generally selected for known boron values or for values which could be reasonably estimated.

Another selection criteria for CYGNUS core calculation time points is xenon. Based on the amount of time points in the core follow data file it is necessary for this validation study to compare data in which the core (and the xenon level) is at equilibrium. Xenon should generally reach an equilibrium state after a few days of steady state operation. Thus it is necessary to choose time points that have been operated at constant power for at least a few days prior. Recent shutdowns or startups will cause xenon transients and lead to a poor comparison with CYGNUS. See previous report (phase 2) for a more detailed discussion of the current xenon model in CYGNUS.

2.2.1 Eigenvalue calculations

Figure 5.2 and Figure 5.3 through Figure 5.12 display the eigenvalue calculated by CYGNUS and other parameters. Note that Figure 5.2 shows more calculated keff values in order to include the data that must be analyzed for the specific dates on the flux maps. The points that deviate

greatly from the critical keff value in the first part of cycle 1A (prior to the long shutdown) can be explained by recent power shifts leading to strong xenon transients that cause the equilibrium xenon assumption to be incorrect.

Figure 5.3 through Figure 5.12 show the power transients in the first part of cycle 1A alongside keff and other operating parameters. In these figures it is clear that stable power values lead to stable keff values, and vice versa. In general the eigenvalue stays within 400 pcm for the entire cycle.

2.2.2 Detector Readings

Table 5.1 shows the flux maps that were available for Ringhals-3 cycle 1A prior to the 5 month shutdown occurring on 21.10.1981. After this date there is a significant drop in keff (discussed in section 2.3.1) and it was concluded that it should be attempted to resolve this issue before comparing to the rest of the TIP data. The dates and times in this table are taken from the core follow data given to IFE by Ringhals. It is these date and time points that are used in the CYGNUS calculation. These points are selected to be as close as possible to the time when the TIP data was measured.

A review of the various flux maps given to IFE by Ringhals was done to determine which maps to compare to the calculated data from CYGNUS. The map numbers in bold face in Table 5.1 were used for comparison. Since accurate boron values are important to a PWR core calculation, some values needed to be interpolated. However, as shown in Figure 5.1 the boron interpolation in the first half of cycle 1A is difficult to predict accurately without a measurement value. The comment column in Table 5.1 helps to explain the reasoning involved in picking a boron value.

Figure 5.13 through Figure 5.36 show the comparison of the relative detector readings measured with the TIP to the readings calculated using CYGNUS for flux maps 7, 9, 18, 20, 21, 22, 23, and 24. For each flux map their are three plots: the core average relative axial reading, the axial reading in the assembly with the maximum measured reading, and assembly average relative radial reading.

2.3 Isotope Tracking Model

Currently the CYGNUS core simulator relies predominately on the HELIOS lattice code for isotopic tracking. Xenon and samarium burnup chains are tracked in CYGNUS on a time-dependent basis. All of the rest of the isotope number densities not included in these two burnup chains are tracked based on burnup using HELIOS.

2.3.1 Keff Drop

Around 21.10.1981 (5991.7 MWd/t) there was a long 5 month shutdown at Ringhals unit 3. Although it is difficult to distinguish the exact reason, Figure 5.7 and Figure 5.37 show that the eigenvalue calculation generally drops by approximately 300 pcm. While in the first part of cycle 1A (prior to the long shutdown) these sort of outlying values could be explained as anomalous behavior resulting from recent power shifts, in the second part of cycle 1A this sort of trend cannot be explained with the same reasoning. This is because the power is much more steady during the second part of the cycle and as shown in Figure 5.1 the boron level is less sporadic. One explanation for this drop in keff is the buildup and decay of numerous isotopes during shutdown that strongly effect core reactivity. Sometimes this is referred to as the shutdown cooling effect.

2.3.2 Important Isotopes

The determination of which isotopes to track must be based on their effect on reactivity in the core. In this sense, the majority of isotopes occurring within the reactor core and generated during fission can likely be ignored. Additionally, some fission products have such a short half

life that they too can be ignored. Listed below are some of the more important decays that will have to be tracked.

$^{135}I \rightarrow {}^{135}Xe$	$T_{1/2}$=6.7h
$^{149}Pm \rightarrow {}^{149}Sm$	$T_{1/2}$=54h
$^{239}Np \rightarrow {}^{239}Pu$	$T_{1/2}$=2.4d
$^{148m}Pm \rightarrow {}^{148}Sm$	$T_{1/2}$=41d
$^{148}Pm \rightarrow {}^{148}Sm$	$T_{1/2}$=2.6y
$^{155}Eu \rightarrow {}^{155}Gd$	$T_{1/2}$=4.7y
$^{241}Pu \rightarrow {}^{241}Am$	$T_{1/2}$=14.4y

This is not a complete listing of all of the necessary decays that must be tracked, but is rather an example of some isotopes that add or subtract reactivity from the core. To determine a complete list of isotopes necessary to be tracked requires a more detailed survey of neutron microscopic cross sections, half lives and fission yields for heavy-metal isotopes, burnable absorber isotopes, fission products, etc.

The creation of Pu-239 is one of the more interesting transmutations during the current shutdown period. Since the shutdown occurs after about 6000 MWd/t of burnup there should be a substantial buildup of Np-239. The current model calculates the core eigenvalue neglecting any reactivity insertion that occurs with the decay of Np-239 to Pu-239. This would thus cause CYGNUS to under predict core criticality. But this is just one isotopic effect that could possibly be disguised by other isotopic effects. Additionally, it is necessary to know how much Np-239 (or other parent nuclides) initially exists at any time in order to be able to model a shutdown at any time. Hence the need for a more detailed isotopic tracking model that can account for not only decay paths, but numerous burnup paths as well.

2.3.3 Improvement of Isotope Tracking Model

The improvement of the isotopic tracking model in CYGNUS begins with a general understanding of burnup in nuclear reactors. The change in number density of a specific nuclide can be understood as:

$$\frac{dN_i}{dt} = production\ rate - absorption\ rate - decay\ rate \tag{2.3.1}$$

In a more detailed way this equation can be described as in Reference [2.5]:

$$\frac{dN_i}{dt} = \sum_j \gamma_{ji}\sigma_{f,j}N_j\phi + \sigma_{c,i-1}N_{i-1}\phi + \sum_k \lambda_k N_k - \sigma_{a,i}N_i\phi - \lambda_i N_i \tag{2.3.2}$$

N_i : number density of nuclide i [cm^{-3}]
γ_{ji} : yield of nuclide j from the fission of nuclide i
$\sigma_{f,j}$: microscopic fission cross section of nuclide j [cm^2]
ϕ : neutron flux [$cm^{-2}s^{-1}$]
$\sigma_{c,i-1}$: capture cross section of nuclide i-1 [cm^2]
$\sigma_{a,i}$: absorption cross section of nuclide i [cm^2]
λ_i : decay constant of nuclide i [s^{-1}]

There are numerous techniques for solving the burnup equation. One technique is the matrix exponential method in which the number density of a specific nuclide as a function of time may be written as the exponential of a "burnup" matrix composed of all terms except for number densities. There are many ways to solve such a problem, one of the more popular tools is the

ORIGEN code. While the matrix exponential method can be fast, it has yet to be regularly used for core simulations.

An alternative method is more of a direct solution of the burnup equation (sometimes called the Bateman method). In this case the individual burnup chains must be examined and linearized as a Markov chain. Figure 5.38 demonstrates this chain linearization in a very general way in which all of the letters represent specific nuclides. Once a proper examination is complete and the burnup chains are written, a general solution to these chains can be described as in Reference [2.6]:

$$\frac{dN_t(t)}{dt} = y_t + g_{t-1}N_{t-1}(t) - l_t N_t(t) \qquad (2.3.3)$$

y_t : general yield term [$cm^{-3}s^{-1}$]
g_{t-1} : general gain term [s^{-1}]
l_t : general loss term [s^{-1}]

The gain (production) and loss (absorption and decay) terms can thus be understood in a simplified manner and the appropriate nuclide densities may be solved as a function of time. These nuclide densities may then be used in a node-wise microscopic depletion model for tracking in CYGNUS.

2.4 Intra-Nodal Burnup Tilt Effect

The neutron cross sections within a node (or an assembly) are dependent on the intra-nodal burnup distribution, which presently is calculated by a lattice code applying the reflective boundary condition at the interface of the node. The reflective boundary condition is applied based on the assumption that the node is surrounded by similar nodes during the burnup (the infinite-lattice assumption). However, this is generally not the case. For example, in the core of Ringhals-3, assemblies with different enrichment are loaded, and at the interface between assemblies of different enrichment, the boundary condition should not be reflective because of the neutron net corrent between these assemblies caused by the mismatch of the neutron spectrum. So the actual intra-nodal burnup distribution is generally different from that of the lattice calculation. This affects the cross sections and consequently, the VNEM coefficients have to be corrected.

We call the difference of the intra-nodal burnup distribution between the lattice burnup calculation and the actual one as the "intra-nodal burnup tilt $T_{nf,\,g,\,nb}$" and define:

$$T_{nf,\,g,\,nb} = E_{nf,\,g,\,nb} - E^{\infty}_{nf,\,g,\,nb} \qquad (2.4.1)$$

where the indices are

nf : fuel rod in the node
g : neutron energy group
nb : burnup step

and

$$E_{nf,\,g,\,nb} = B_{nf,\,g,\,nb} / B^{n}_{nb} \qquad (2.4.2)$$
$$E^{\infty}_{nf,\,g,\,nb} = B^{\infty}_{nf,\,g,\,nb} / B^{n}_{nb} \qquad (2.4.3)$$

where

$B_{nf, g, nb}$: group-wise burnup of fuel rod nf at burnup step nb, i.e., produced cumulative energy by fissions induced by neutrons of group g in fuel rod nf until burnup step nb divided by the initial smeared density of the heavy elements in the node

$B^{\infty}_{nf, g, nb}$: same as $B_{nf, g, nb}$, but for the infinite-lattice case

and

$$B^{n}_{nb} = \sum_{nf, g} B_{nf, g, nb} = \sum_{nf, g} B^{\infty}_{nf, g, nb} \qquad (2.4.4)$$

is the nodal burnup. Here we define the intra-nodal burnup tilt when the nodal infinite-lattice burnup is equal to the actual nodal burnup as shown in this equation.

2.4.1 Calculation of Intra-Nodal Burnup Tilt

One of the merits of VNEM is that we can calculate the intra-nodal burnup tilt without making any additional assumptions or approximations.

The equations for the source and the boundary expansion coefficients for each of all the parameters g, nr become, in the case of the infinite-lattice, from Eqs.(A.2.14) and (A.3.16) of Reference [2.3]:

$$\begin{aligned} & F^{S}_{nr=1, g}\, ANN_{nr=1, nr'=1; g} \\ &= \sum_{g'} (F^{S}_{nr'=1, g'}\, ANNS_{nr=1, nr'=1; g, g'} + \sum_{pp, lmc} F^{CB}_{pp, lmc, g'}\, ANCS_{nr=1, pp, lmc; g, g'}) \\ &\quad + (1 / \lambda) \chi_{g} \sum_{g'} (F^{S}_{nr'=1, g'}\, ANNF_{nr=1, nr'=1; g, g'} + \sum_{pp, lmc} F^{CB}_{pp, lmc, g'}\, ANCF_{nr=1, pp, lmc; g, g'}) \end{aligned} \qquad (2.4.5)$$

$$\begin{aligned} & - F^{S}_{nr=1, g}\, JCN_{pp, lmc, nr=1, g} - \sum_{pp', lmc'} F^{CB}_{pp', lmc', g}\, JCC_{pp, lmc, pp', lmc', g} \mid \text{left node} \\ &= F^{S}_{nr=1, g}\, JCN_{pp, lmc, nr=1, g} + \sum_{pp', lmc'} F^{CB}_{pp', lmc', g}\, JCC_{pp, lmc, pp', lmc', g} \mid \text{right node} \end{aligned} \qquad (2.4.6)$$

Equations (2.4.5 and 6) is obtained by using the facts:

(1) The infinite lattice is a 2-dimensional (radial-cross sectional of an assembly) problem
(2) Imaginary part = 0 at the reflective boundary of the infinite-lattice
(3) Higher spatial mode = 0 for the infinite-lattice problem

These equations can be solved node by node without spending much computing time and we can obtain the infinite-lattice scalar flux distribution within a node. From this scalar flux we can readily calculate the group-wise power density distribution and the burnup distribution $B^{\infty}_{nf, g, nb}$ (see 2.4.3) within a node for infinite-lattice case.

As for the actual burnup distribution $B_{nf, g, nb}$ (see 2.4.2), CYGNUS calculates the "actual" scalar flux distribution to obtain the rod-by-rod power density. Therefore, $B_{nf, g, nb}$ can be obtained as a byproduct of normal calculation of CYGNUS. Thus we obtain the intra-nodal burnup tilt from Eq.(2.4.1).

We also have developed a method to estimate the effect of the intra-nodal burnup tilt on the VNEM coefficients[2.4]. This effect obviously increases almost monotonically as the burnup increases. In a preliminary numerical work[2.4] by using NEACRP MOX benchmarking problem, the intra-nodal burnup tilt effect on VNEM results is significant for nodal burnup >

~5000MWD/T. However, in the case of Ringhals-3, Cycle 1A, it seems that this effect cannot be observed up to the core average burnup of 10,000MWD/T. Therefore we have to postpone the test of the method for the subsequent cycles, which is planned to be performed in the next year.

2.5 References

[2.1] M. Tsuiki, Steven Mullet and W. H. Beere: "Comparison of VNEM to Measured Data from Ringhals Unit 3 (Phase 2)," AR-CYGNUS-NKS-01-09, 2009.

[2.2] F. D. Giust, R. J. J. Stamm'ler, and A. A. Ferri: "HELIOS1.7 User Guide and Manual," Studsvik and Scandpower, 2001.

[2.3] M. Tsuiki and W. H. Beere: "Comparison of VNEM to Measured Data from Ringhals Unit 3 (IACIP)," AR-VNEM-NKS-R-01-08, 2008.

[2.4] W. H. Beere: "The effect of exposure on pin power calculations in multi-assembly nodal codes." XII Meeting on "Reactor Physics Calculations in The Nordic Countries," Halden, 2005.

[2.5] D. G. Cacuci: *Handbook of Nuclear Engineering*, 1st Ed., Springer, 2010.

[2.6] R. J. J. Stamm'ler and M. J. Abbate: *Methods of Steady-State Reactor Physics in Nuclear Design*, Academic Press, London.

3 Numerical Benchmarking of VNEM for BWR

VNEM has been tested mainly for PWR cores so far. As the first step of applying VNEM to BWR cores we made numerical benchmark calculations of BWR system as we did for PWR case by imitating NEACRP MOX benchmark problems[3.1].

3.1 Benchmark Problem

Figure 5.39 shows the geometry of the assembly used in the benchmarks. Each of the regions in the assembly, including each fuel cell, is homogenized. The regions are divided by several space meshes. The meshes along x-direction is shown in the figure. The same meshes are used also along y-direction. With this same geometry we made 2 types of assemblies (fuel types 1 and 2). Here type 1 is a high-enriched and type 2, a low enriched fuel assemblies, respectively.

Table 5.2 shows the macro cross sections of representative regions for the normal fuel cell, the fuel cell with the burnable poison, the water rod, the gap water, and the homogenized gap water with the channel box for fuel types 1 and 2. Three energy groups are used.

The macro cross sections and the size of the regions in the assembly are taken from a typical BWR assembly and are rounded because there is no need for many digits of these figures.

Imitating cases 2 and 5 of NEACRP MOX benchmark problems, we made cases 1 and 2 as shown in Figure 5.40. Both cases are 2-dimensional (2D) problems. Here case 1 is a radial infinite system of 4 assemblies. While in case 2 the assemblies in case 1 are surrounded by a water reflector.

3.2 Method

The method of benchmarking is the same as used in Reference [3.1]. The reference solution is calculated by using IFE's reference 2D transport code FCM2D which is based on the method of characteristics (MOC). The parameters used in FCM2D are listed in Table 5.3.

The VNEM coefficients are generated by FCM2D and VCOEF3D in the way described in Reference [2.3]. The parameters used in VCOEF3D-VNEM3D are listed in Table 5.4. Here it should be noted that the source expansion is the same as the case of PWR for nr = 1 through 6. However for nr = 7 and 8 we use 4th order polynomials in the case of BWR while it was 3rd order polynomials in the case of PWR. This may be related to the existence of the water gap around the fuel bundle of a BWR.

The boundary value expansion sr = 1, 2, 3 and the PL order are the same as the PWR case.

3.3 Results

Table 5.5 shows the comparison of the core eigenvalue (the effective multiplication factor, k_{eff}). Both in cases 1 and 2 the errors of VNEM3D to FCM2D are less than 0.1% (100PCM). Table 5.6 shows the comparison of the relative nodal power of VNEM3D to FCM2D, and Table 5.7, the maximum fuel cell power relative to the core average.

As shown in these tables, the agreement of VNEM3D to FCM2D is almost the same as the case of PWR. The error of k_{eff} is less than 0.1%. The errors of nodal powers and the maximum fuel cell powers are less than 2%.

In the case of the BWR the cruciform control blade has strong heterogeneity and cause a rapid spatial change of neutron angular fluxes. Therefore it is very interesting to test VNEM for cases with the control blade inserted. This will be performed in the next year if this project continues.

3.4 Reference

[3.1] M. Tsuiki and W. H. Beere, "A variational nodal transport method for pressurized water reactor core calculations", M&C2005, Avignon, France, 12-15 September, 2005.

4 Conclusions and Future Plan

Comparisons were made of a PWR core simulator CYGNUS with VNEM neutronics module to measured data from Ringhals-3, cycle 1A. The conclusions are summarized as:

1. The agreement of the neutron detector readings is excellent throughout the cycle.
2. The critical eigenvalues are excellent (0.99937 ± 0.00086) before the intermediate long term shutdown, however it drops after the shutdown (0.99647 ± 0.00029).
3. The intra-nodal burnup tilt effect was not significant in this cycle.

To improve above 2, we have started to implement a tracking model for some important isotopes. We expect that we can show improved results in the next phase of this project.

To see the intra-nodal burnup tilt effect we have to extend the core follow calculations to farther cycles (item 3 above). We will perform this also in the next phase.

To investigate the applicability of VNEM to a BWR core, numerical benchmark problems were made just as we did for a PWR core. The results were quite similar to those for PWR cases, i.e. the agreement of VNEM to the reference code (FCM2D - a reference transport code based on the method of characteristics) was as good as PWR cases.

In the next phase we will extend the comparisons to include the cases with cruciform control blade inserted.

5 Tables and Figures

5.1 Tables and Figures for Chapter 2

Table 5.1: List of all flux maps prior to long shutdown for cycle 1A

Map	Date	Time	Comments
7	04.11.1980	0629	Also analyzed in 2009 report with slightly different assumptions.
8	04.11.1980		Same date as map 7. This map is not analyzed.
9	20.12.1980	0600	Also analyzed in 2009 report with slightly different assumptions.
10			Likely the same date as map 9. This map is not analyzed.
11	21.12.1980		Incomplete flux map.
12	21.12.1980	1700	Measurement reading contains too much asymmetry. This map is not analyzed.
13	16.01.1981		Incomplete - this map is not analyzed.
14	16.01.1981		Incomplete - this map is not analyzed.
15	16.01.1981		Incomplete - this map is not analyzed.
16	16.01.1981		Incomplete - this map is not analyzed.
17	17.01.1981	2300	Unknown core status. D-bank position disagrees with core follow. This map is not analyzed.
18	02.02.1981	1200	Interpolated boron value to 974 ppm.
19	19.02.1981	0000	Incomplete. No common thimble measurement - calibration impossible.
20	07.04.1981	0800	Used boron value of 850 ppm from flux map.
21	21.05.1981	0700	Used previous known boron value of 910 ppm.
22	07.08.1981	1500	Used boron value of 777 ppm from flux map.
23	02.09.1981	0700	Boron value of 731 ppm given in core follow data.
24	24.09.1981	0700	Interpolated boron value to 686 ppm.

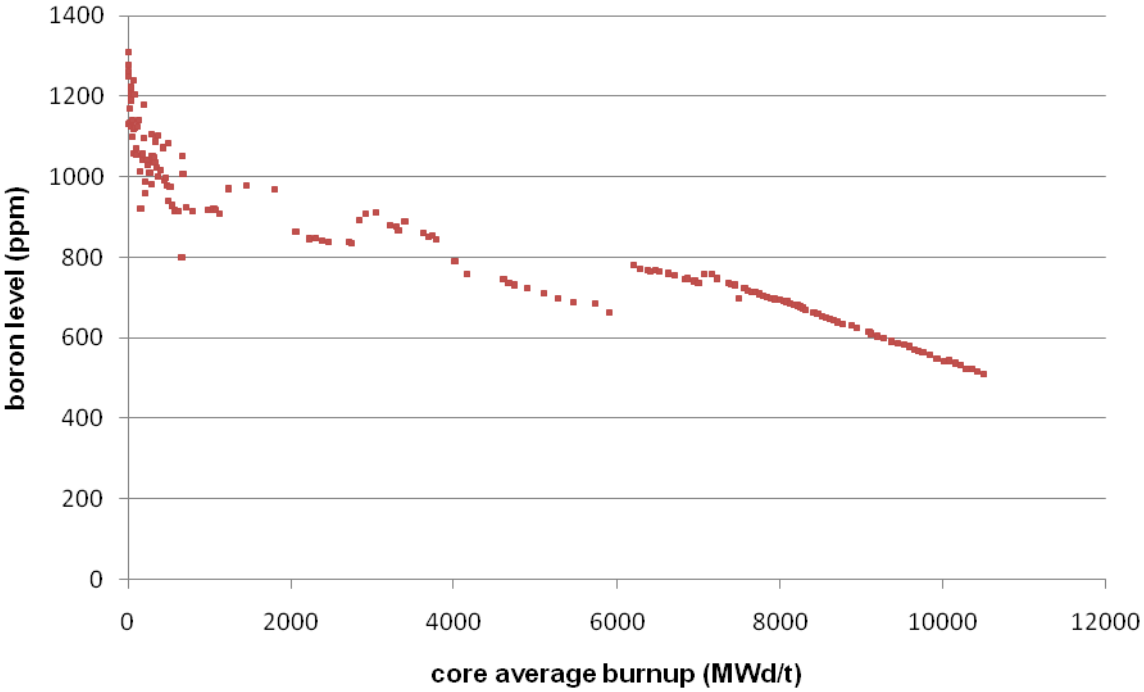

Figure 5.1: Cycle 1A boron vs. burnup

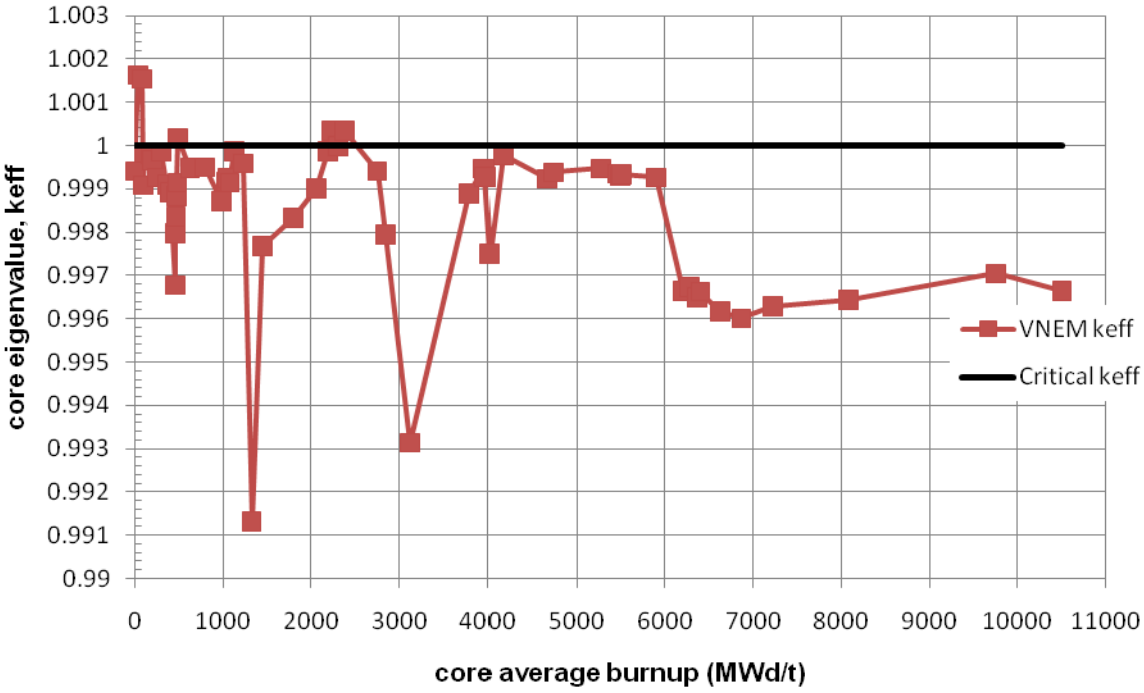

Figure 5.2: Cycle 1A keff vs. burnup

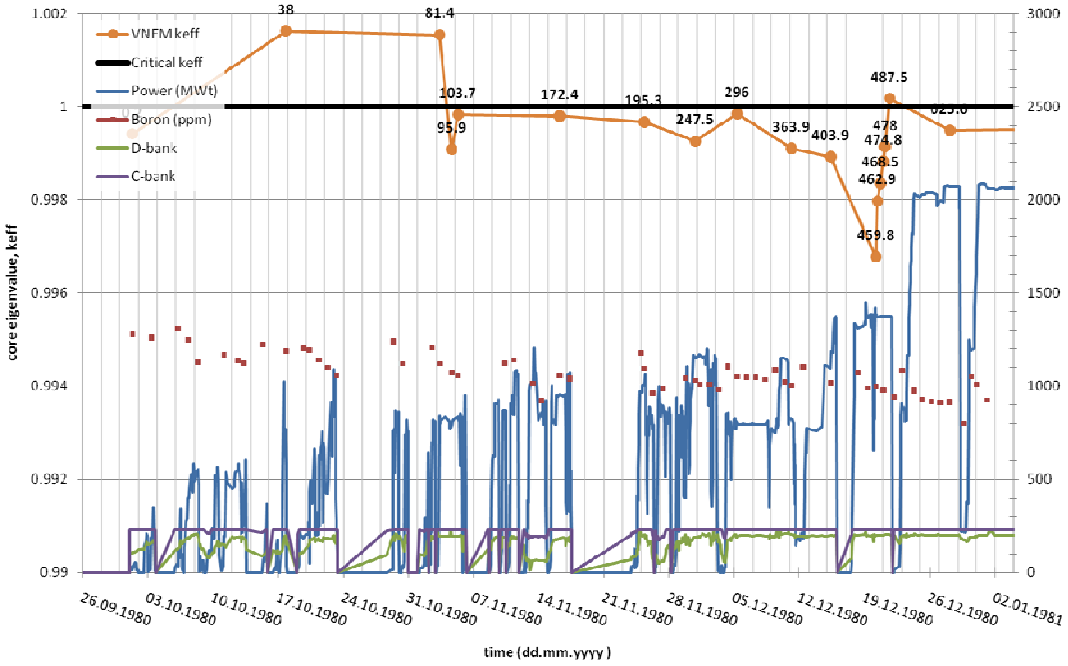

Figure 5.3: VNEM keff and Ringhals-3 cycle 1A operating parameters vs. time

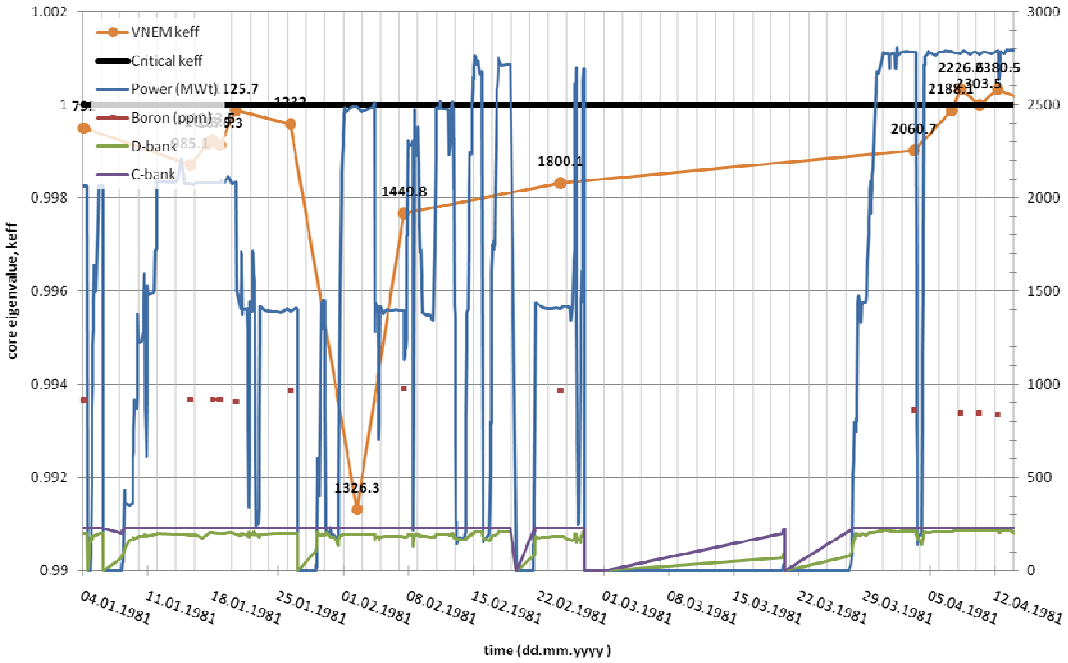

Figure 5.4: VNEM keff and Ringhals-3 cycle 1A operating parameters vs. time

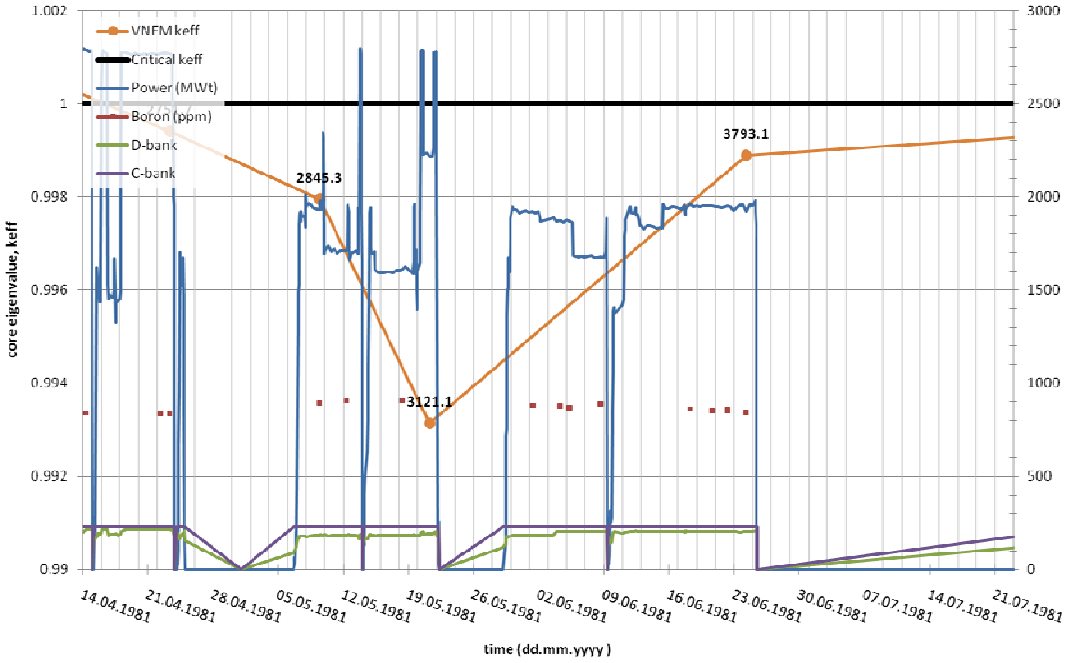

Figure 5.5: VNEM keff and Ringhals-3 cycle 1A operating parameters vs. time

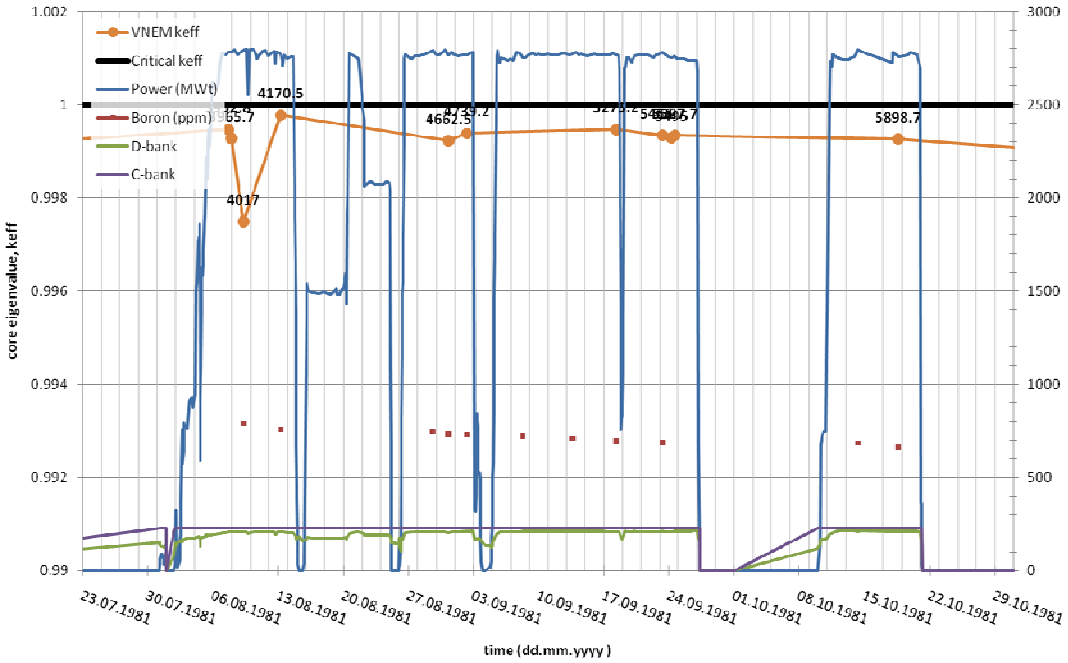

Figure 5.6: VNEM keff and Ringhals-3 cycle 1A operating parameters vs. time

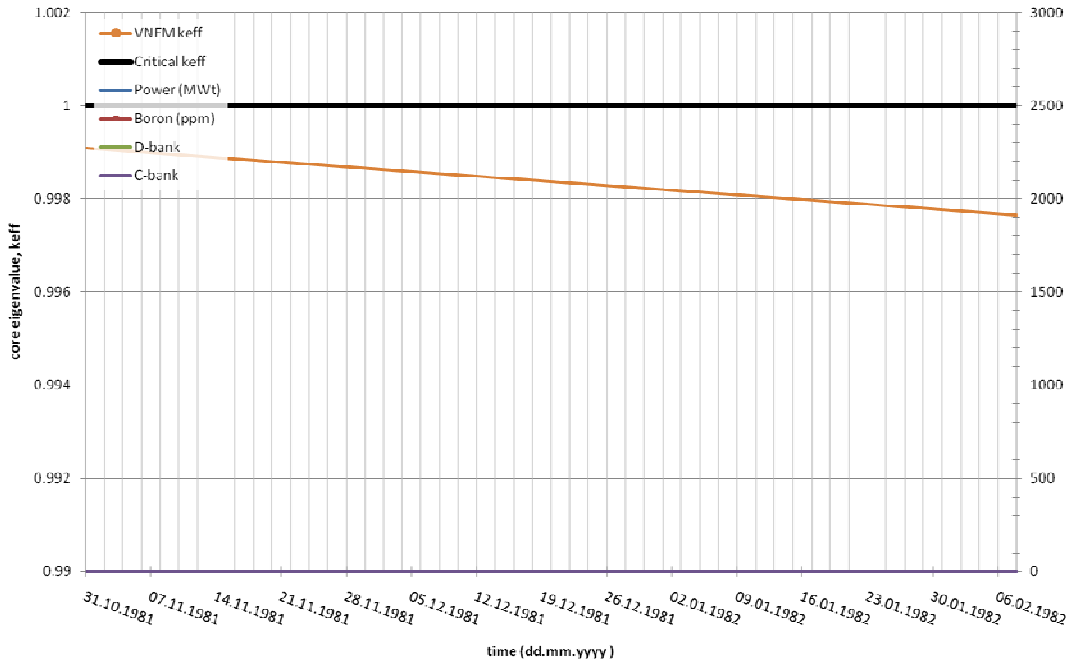

Figure 5.7: VNEM keff and Ringhals-3 cycle 1A operating parameters vs. time

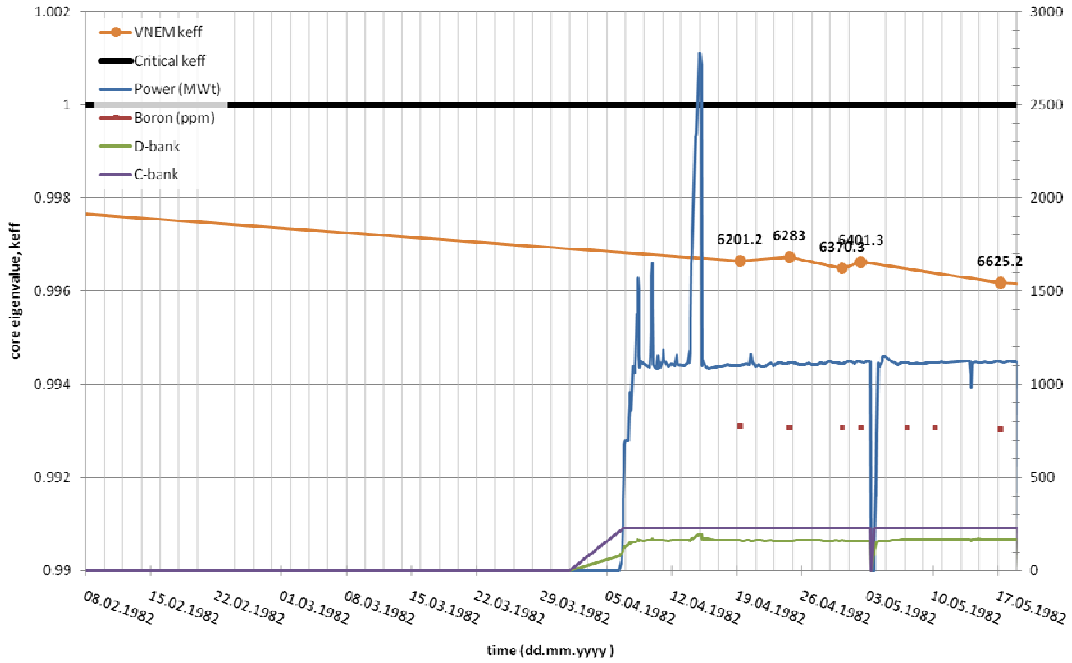

Figure 5.8: VNEM keff and Ringhals-3 cycle 1A operating parameters vs. time

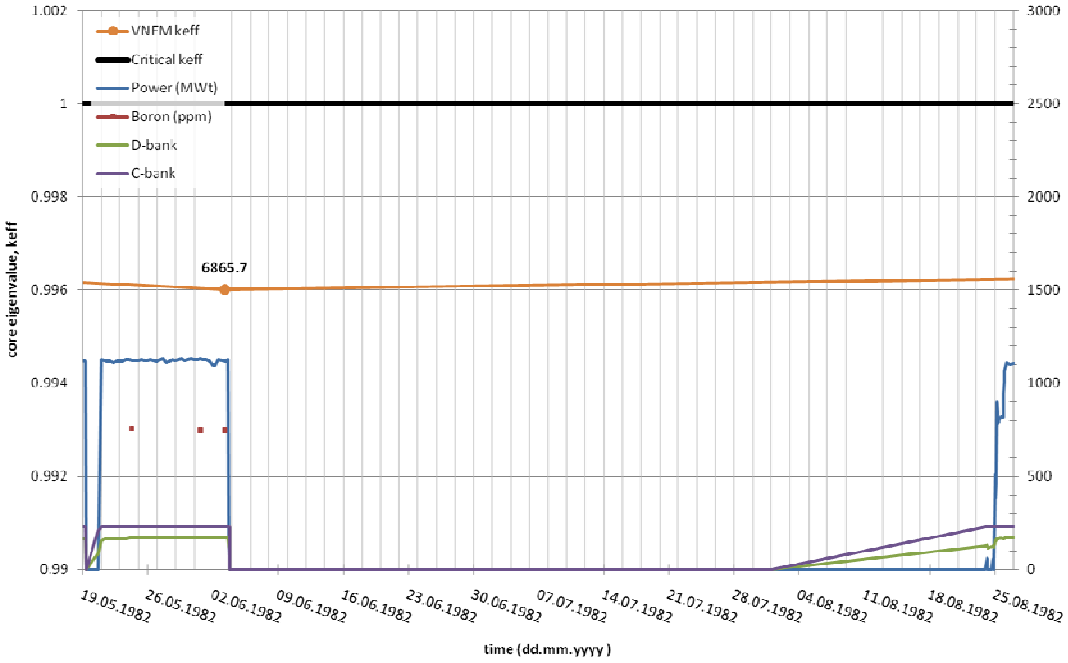

Figure 5.9: VNEM keff and Ringhals-3 cycle 1A operating parameters vs. time

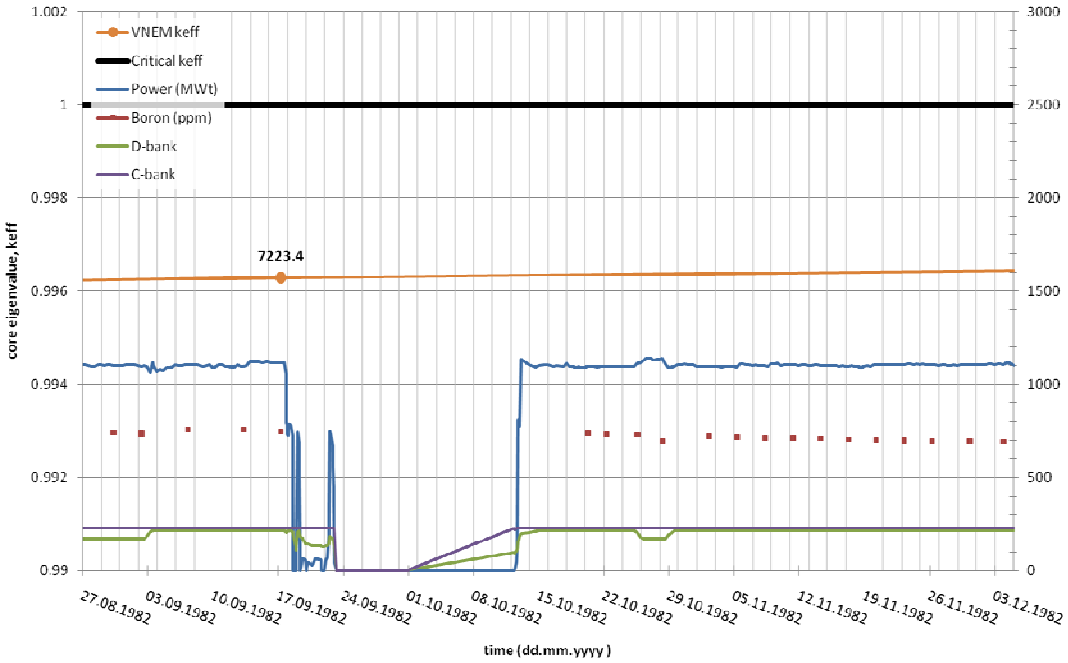

Figure 5.10: VNEM keff and Ringhals-3 cycle 1A operating parameters vs. time

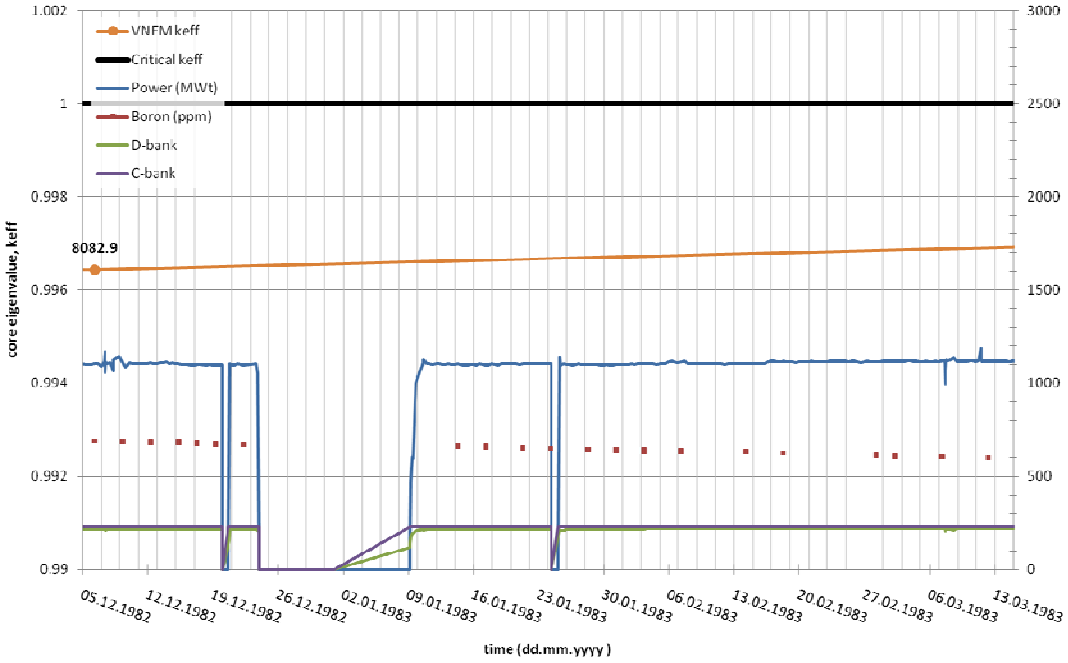

Figure 5.11: VNEM keff and Ringhals-3 cycle 1A operating parameters vs. time

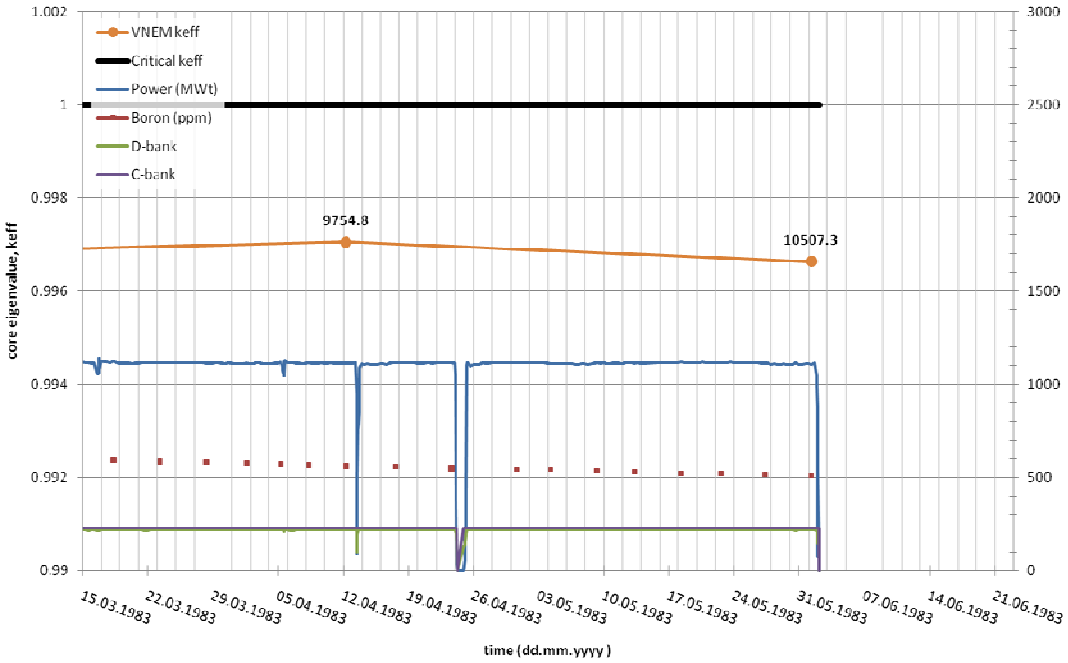

Figure 5.12: VNEM keff and Ringhals-3 cycle 1A operating parameters vs. time

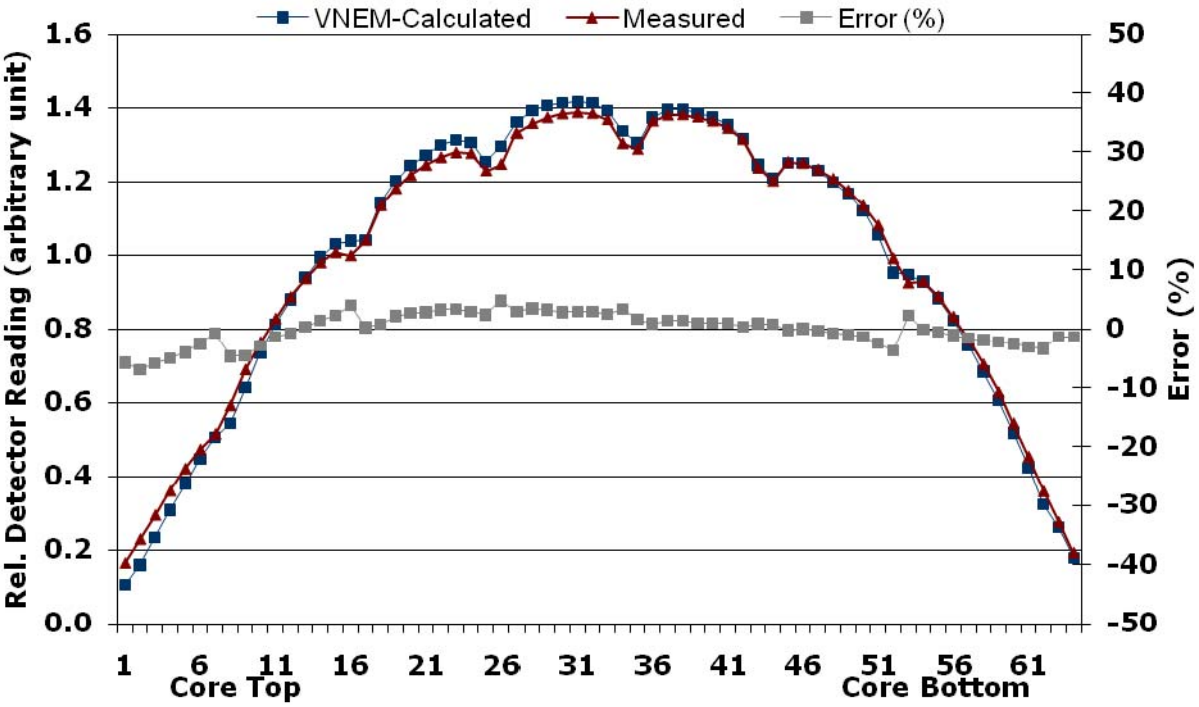

Figure 5.13: Comparison of core average axial detector readings, map 7. The readings are relative to their average.

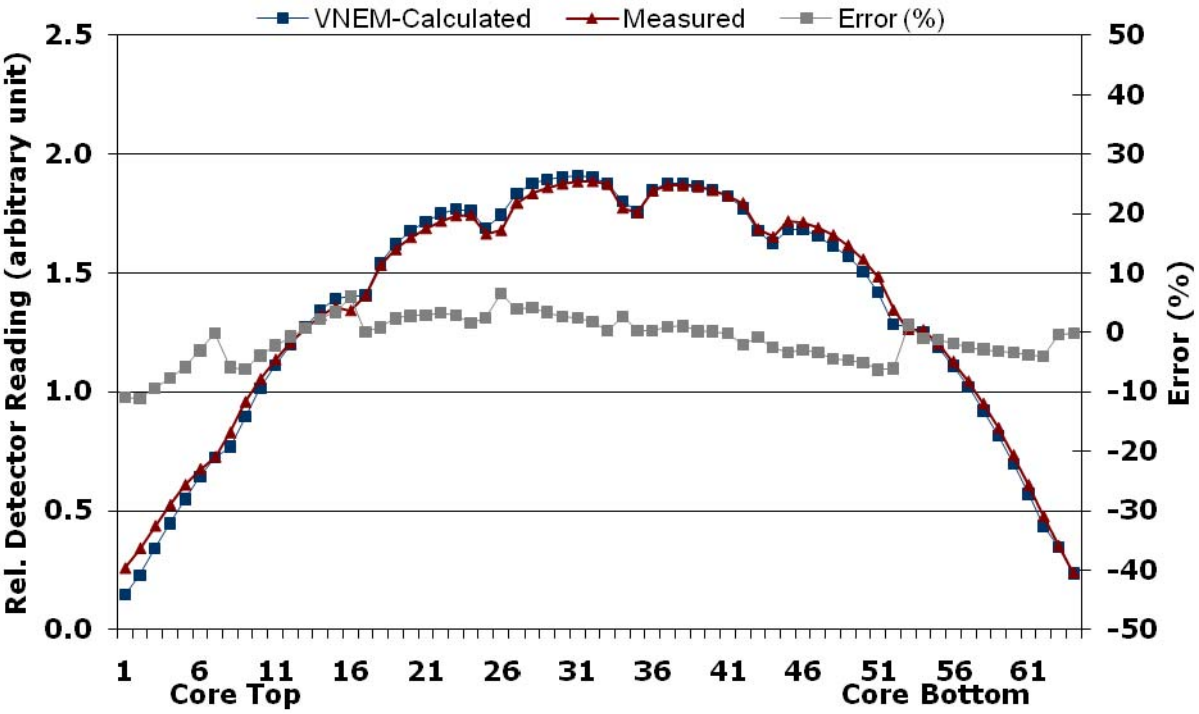

Figure 5.14: Comparison of detector readings in assembly H4, where the maximum reading is observed in map 7. The readings are relative to their average over all the measured positions in the core.

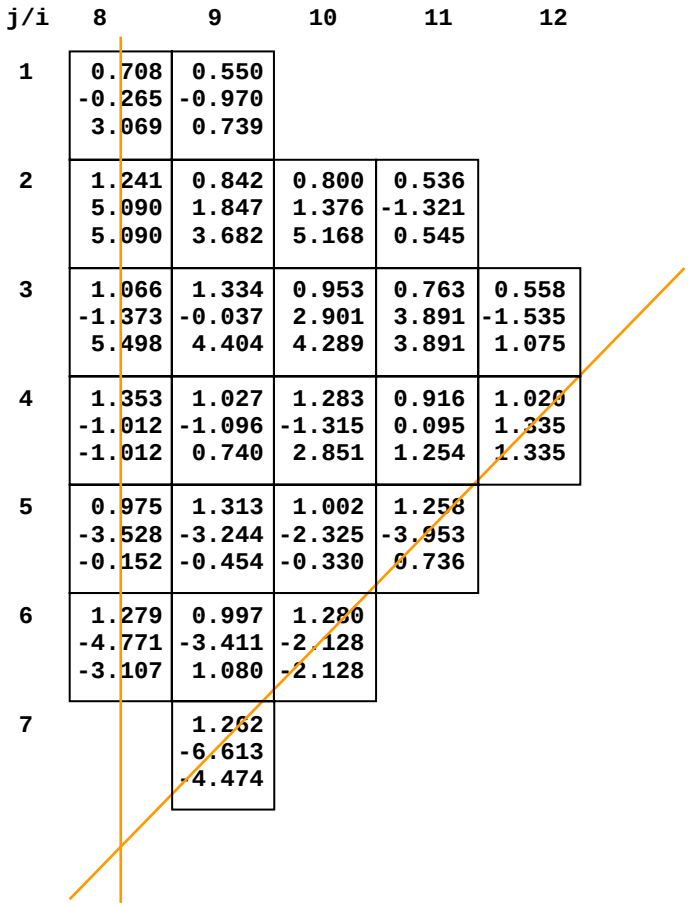

Figure 5.15: Comparison of assembly average radial detector readings, map 7. The readings are relative to their average.

Line 1: Calculated reading by CYGNUS
Line 2: CYGNUS – Upper bound of measured in %
Line 3: CYGNUS – Lower bound of measured in %

The upper and the lower bounds are taken from the maximum and the minimum readings of assemblies at octant-symmetric positions.

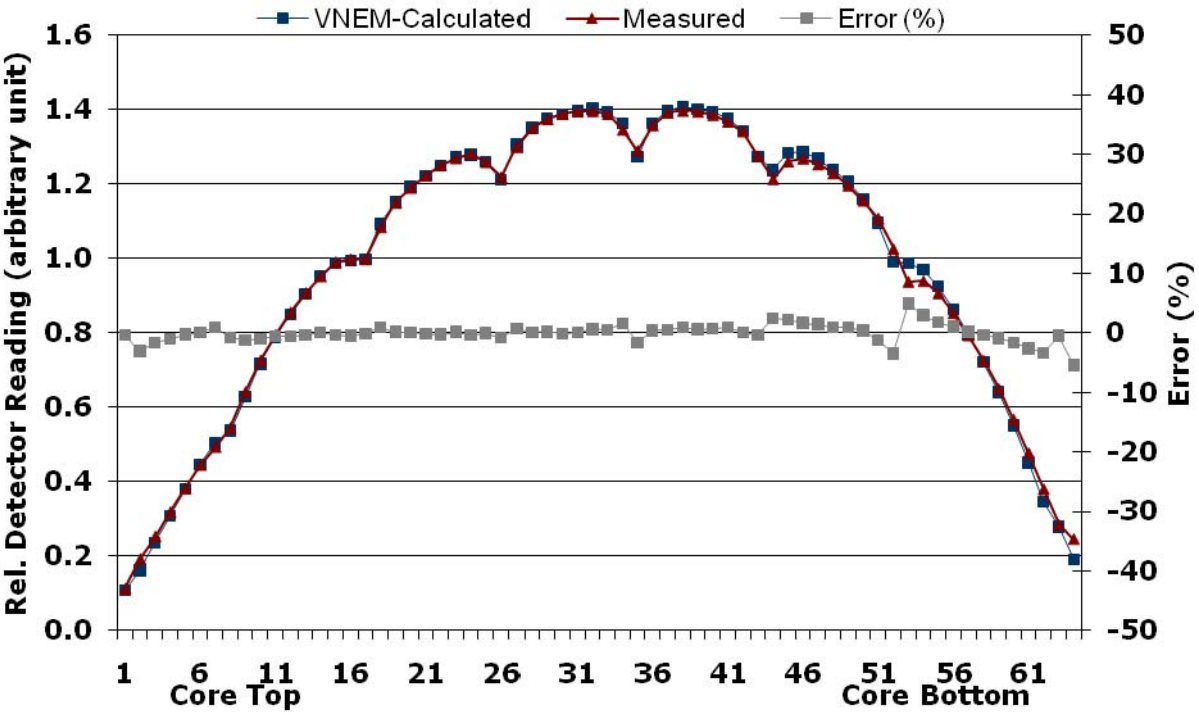

Figure 5.16: Comparison of core average axial detector readings, map 9. The readings are relative to their average.

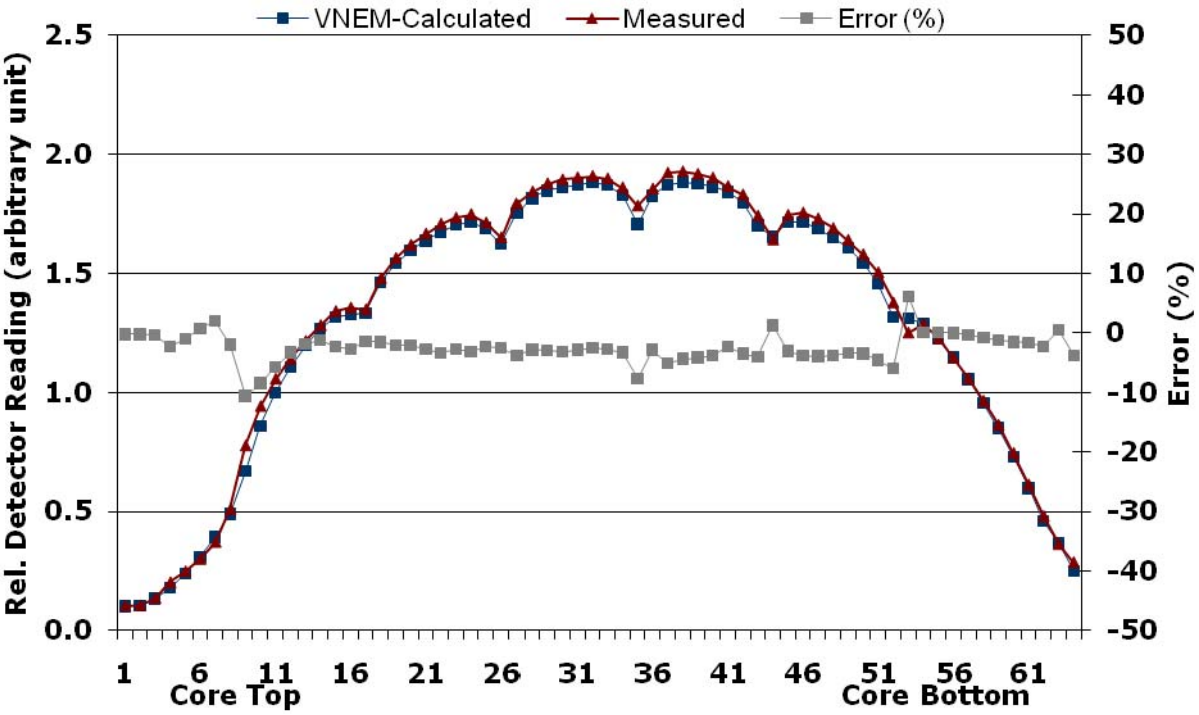

Figure 5.17: Comparison of detector readings in assembly F6, where the maximum reading is observed in map 9. The readings are relative to their average over all the measured positions in the core.

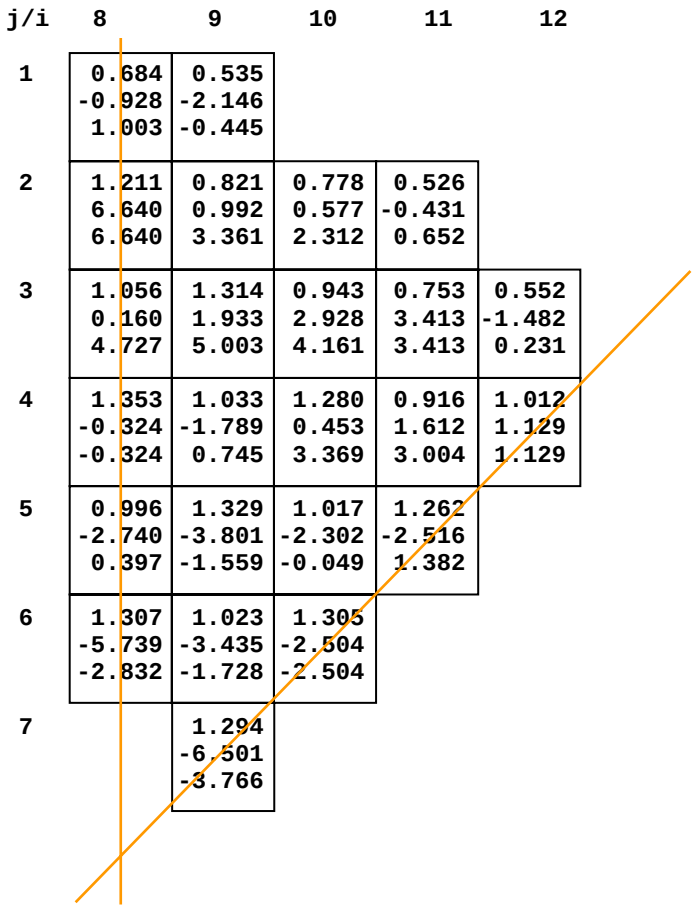

Figure 5.18: Comparison of assembly average radial detector readings, map 9. The readings are relative to their average.

Line 1: Calculated reading by CYGNUS
Line 2: CYGNUS – Upper bound of measured in %
Line 3: CYGNUS – Lower bound of measured in %

The upper and the lower bounds are taken from the maximum and the minimum readings of assemblies at octant-symmetric positions.

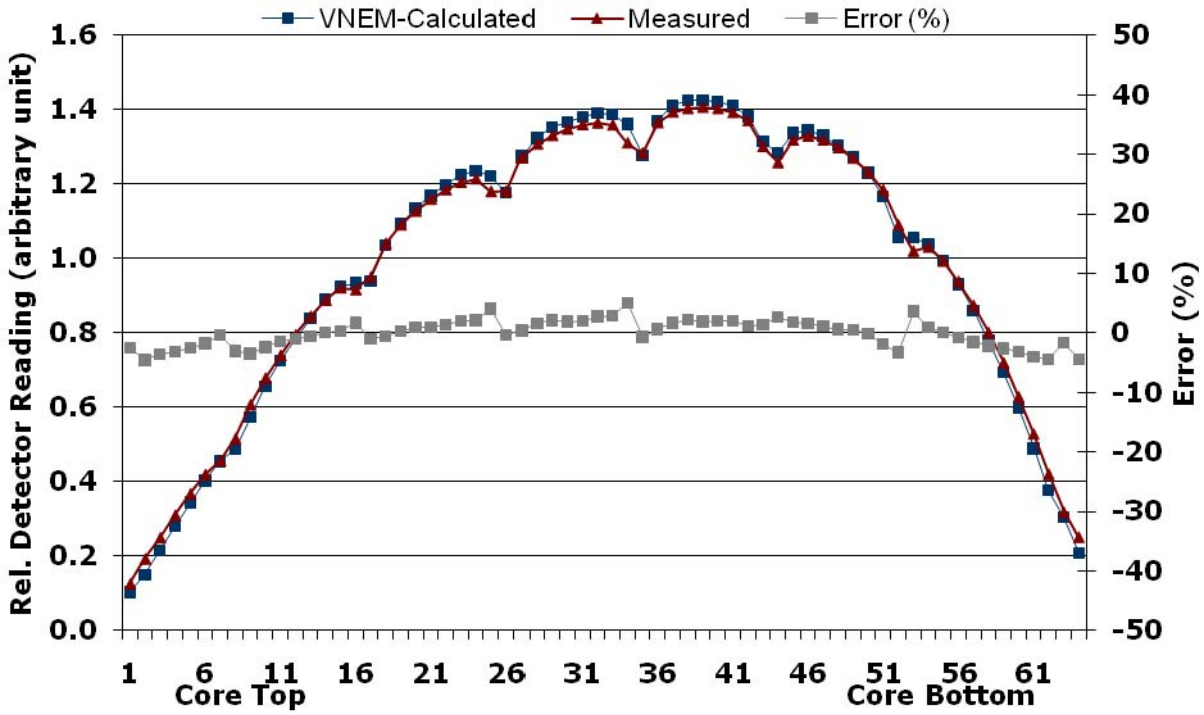

Figure 5.19: Comparison of core average axial detector readings, map 18. The readings are relative to their average.

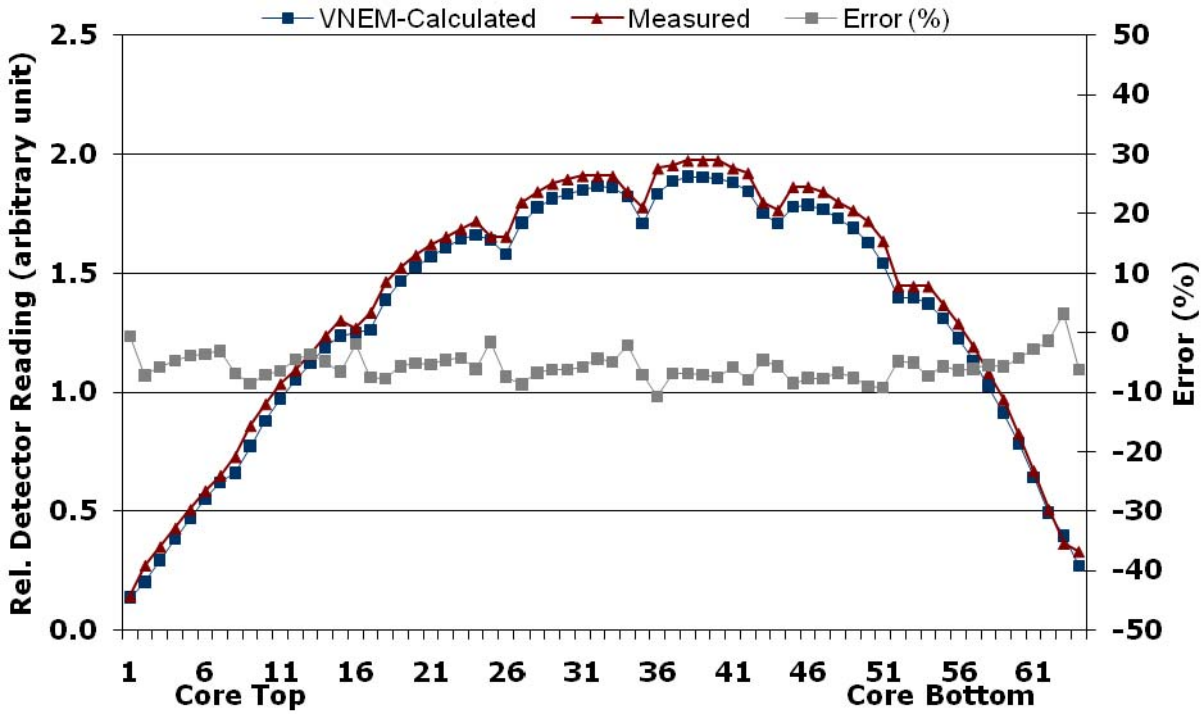

Figure 5.20: Comparison of detector readings in assembly G9, where the maximum reading is observed in map 18. The readings are relative to their average over all the measured positions in the core.

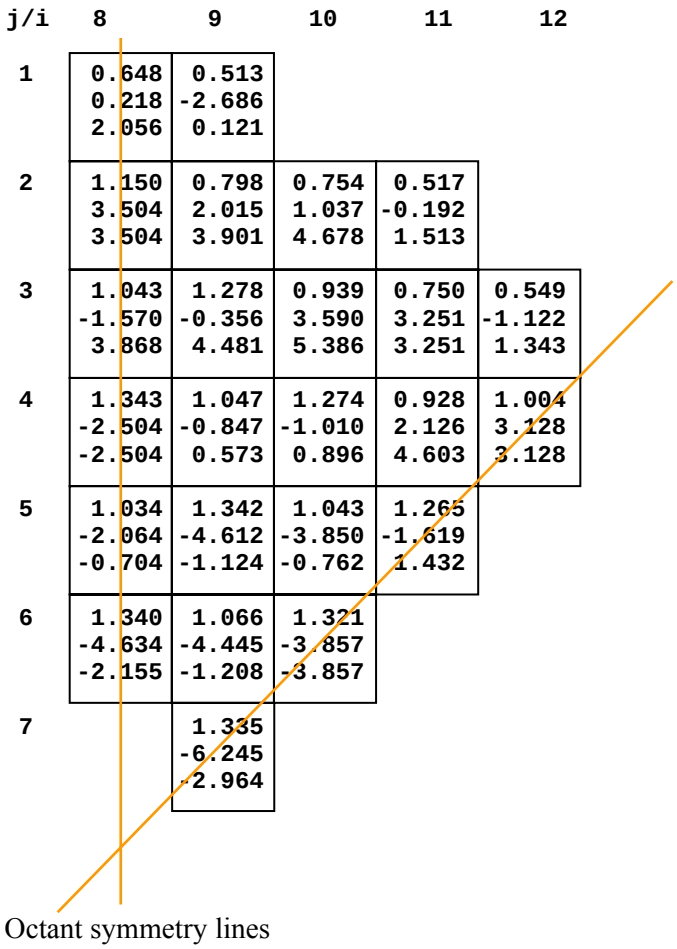

Figure 5.21: Comparison of assembly average radial detector readings, map 18. The readings are relative to their average.

Line 1: Calculated reading by CYGNUS
Line 2: CYGNUS – Upper bound of measured in %
Line 3: CYGNUS – Lower bound of measured in %

The upper and the lower bounds are taken from the maximum and the minimum readings of assemblies at octant-symmetric positions.

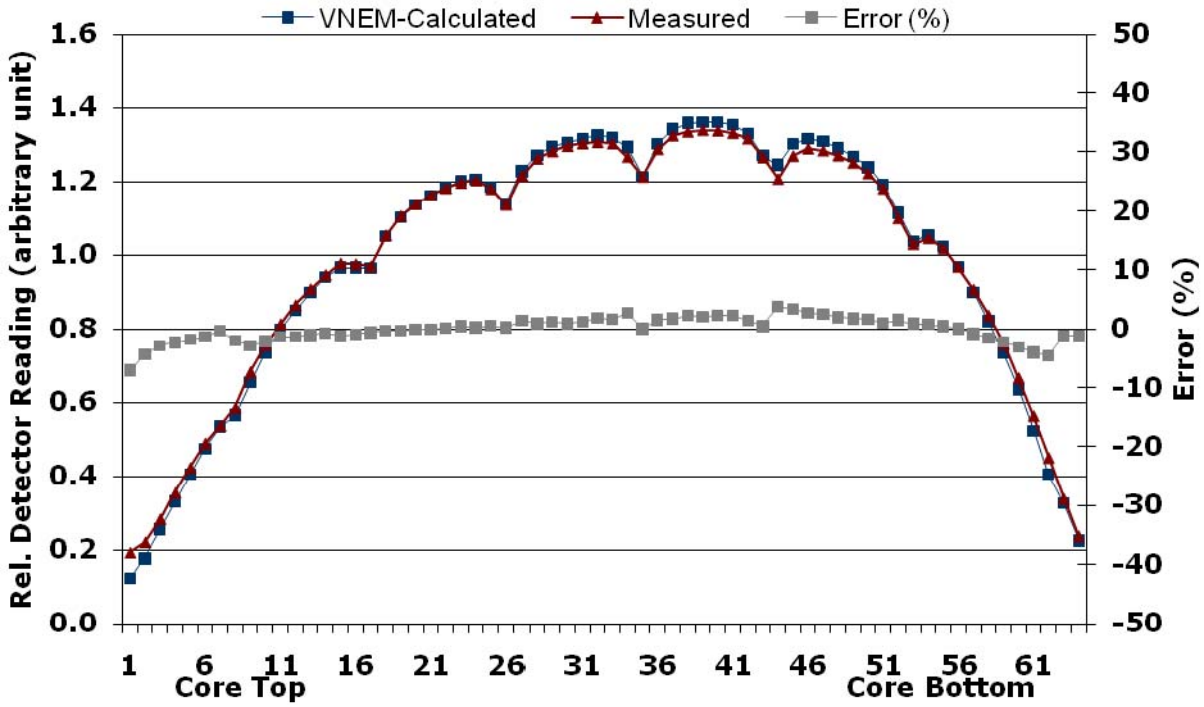

Figure 5.22: Comparison of core average axial detector readings, map 20. The readings are relative to their average.

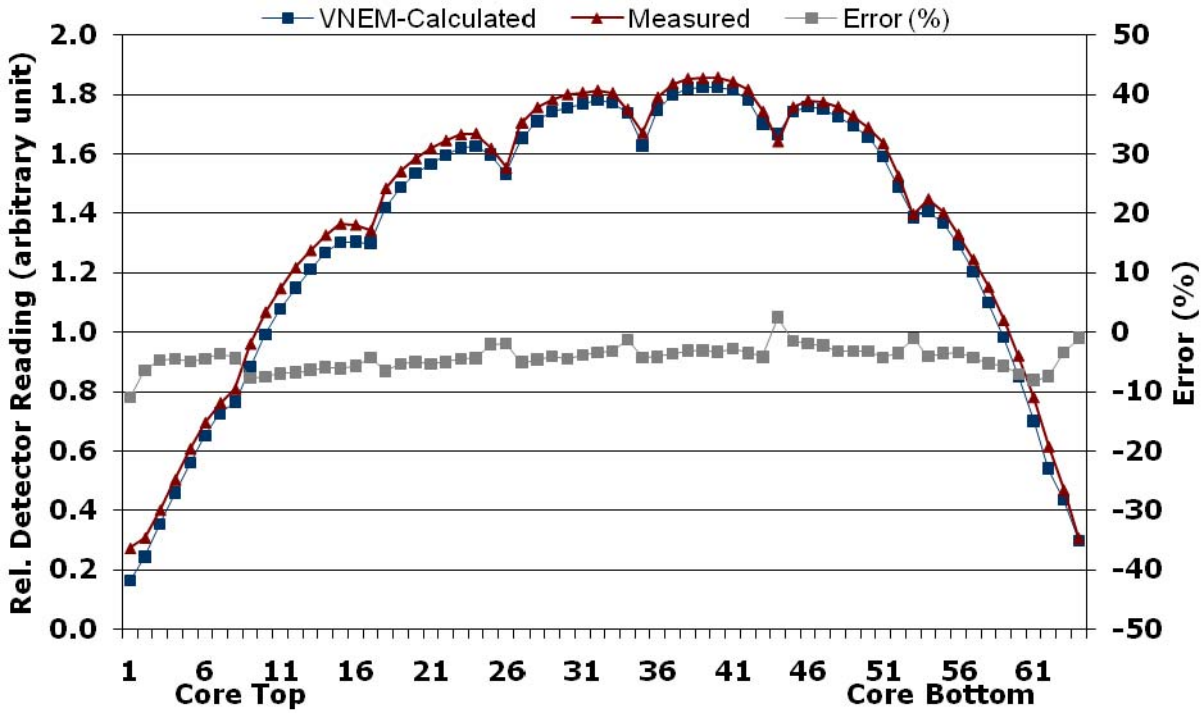

Figure 5.23: Comparison of detector readings in assembly G9, where the maximum reading is observed in map 20. The readings are relative to their average over all the measured positions in the core.

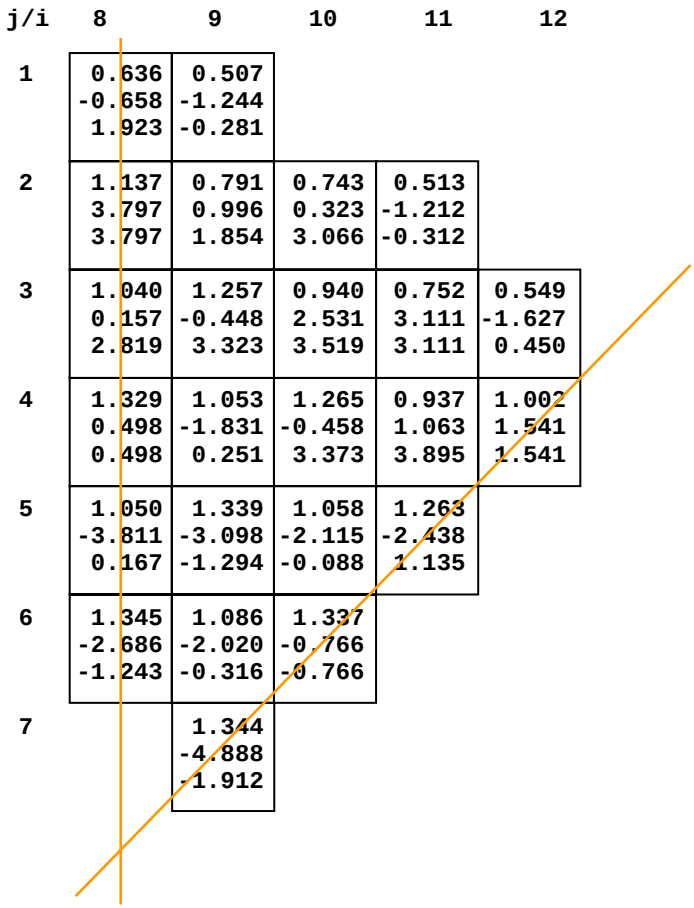

Figure 5.24: Comparison of assembly average radial detector readings, map 20. The readings are relative to their average.

Line 1: Calculated reading by CYGNUS
Line 2: CYGNUS – Upper bound of measured in %
Line 3: CYGNUS – Lower bound of measured in %

The upper and the lower bounds are taken from the maximum and the minimum readings of assemblies at octant-symmetric positions.

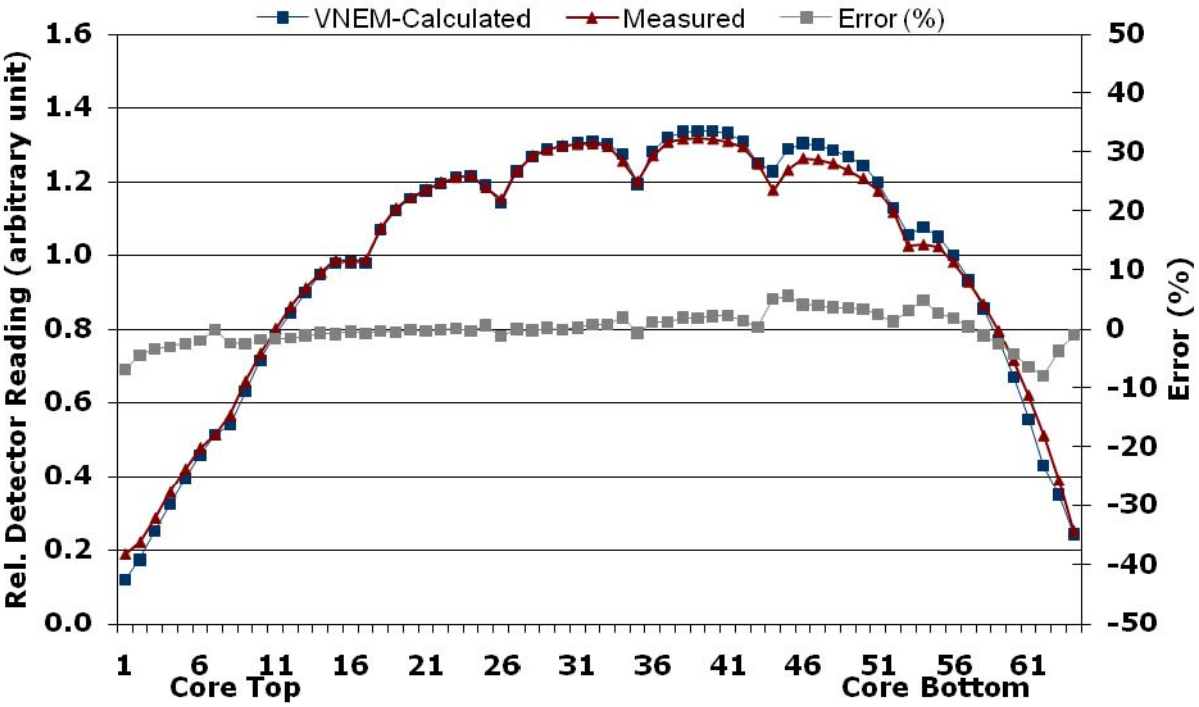

Figure 5.25: Comparison of core average axial detector readings, map 21. The readings are relative to their average.

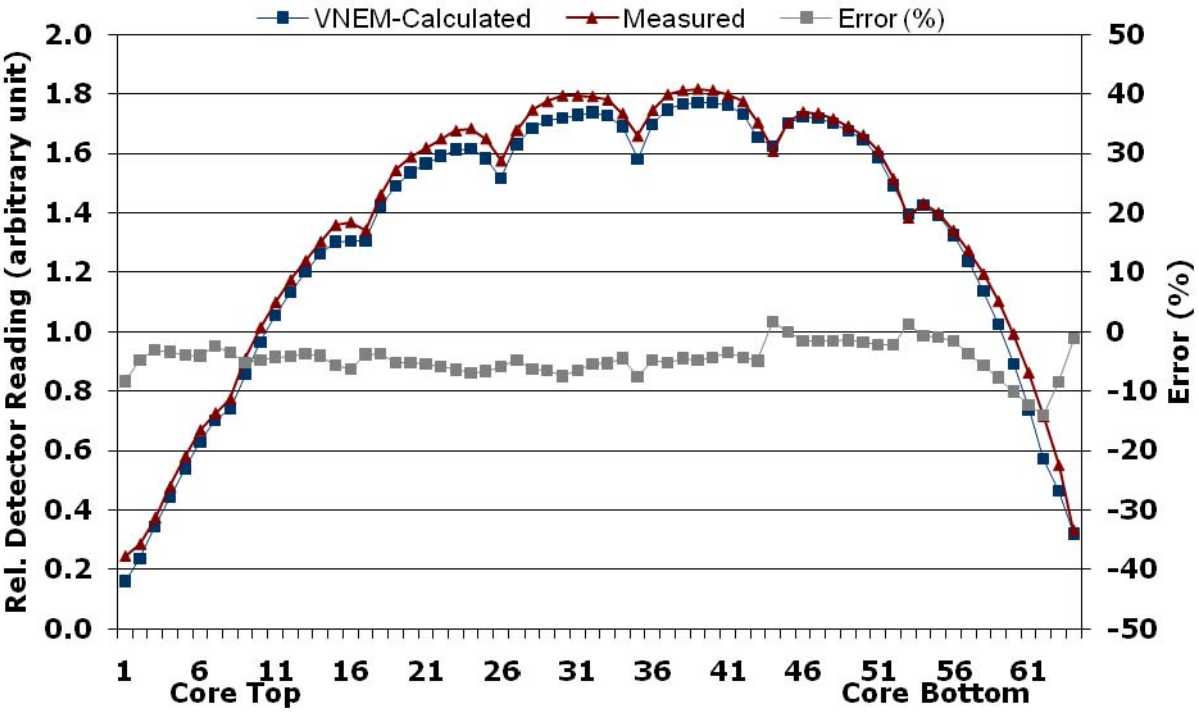

Figure 5.26: Comparison of detector readings in assembly G9, where the maximum reading is observed in map 21. The readings are relative to their average over all the measured positions in the core.

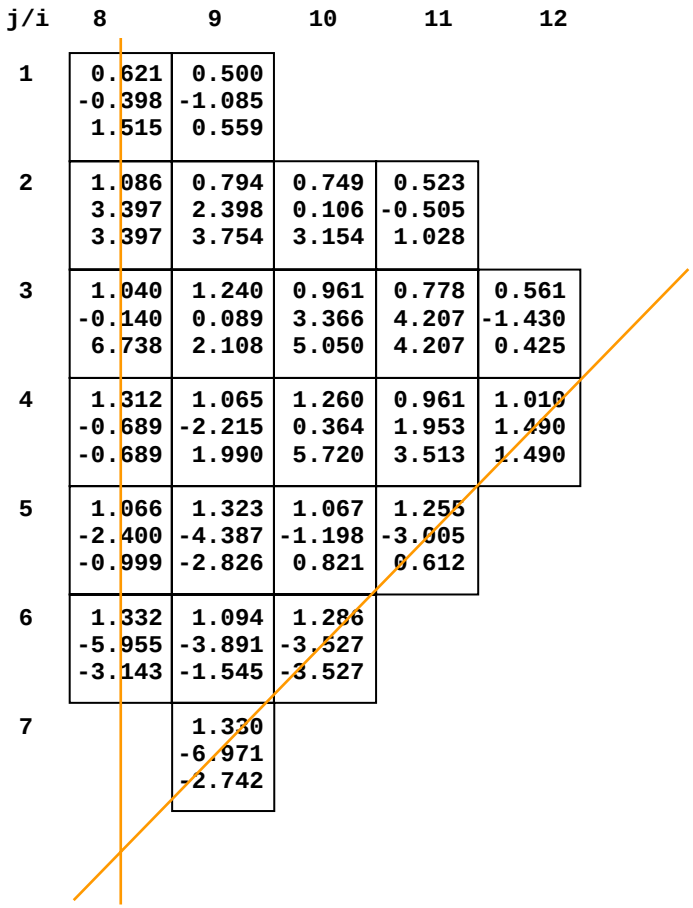

Figure 5.27: Comparison of assembly average radial detector readings, map 21. The readings are relative to their average.

Line 1: Calculated reading by CYGNUS
Line 2: CYGNUS – Upper bound of measured in %
Line 3: CYGNUS – Lower bound of measured in %

The upper and the lower bounds are taken from the maximum and the minimum readings of assemblies at octant-symmetric positions.

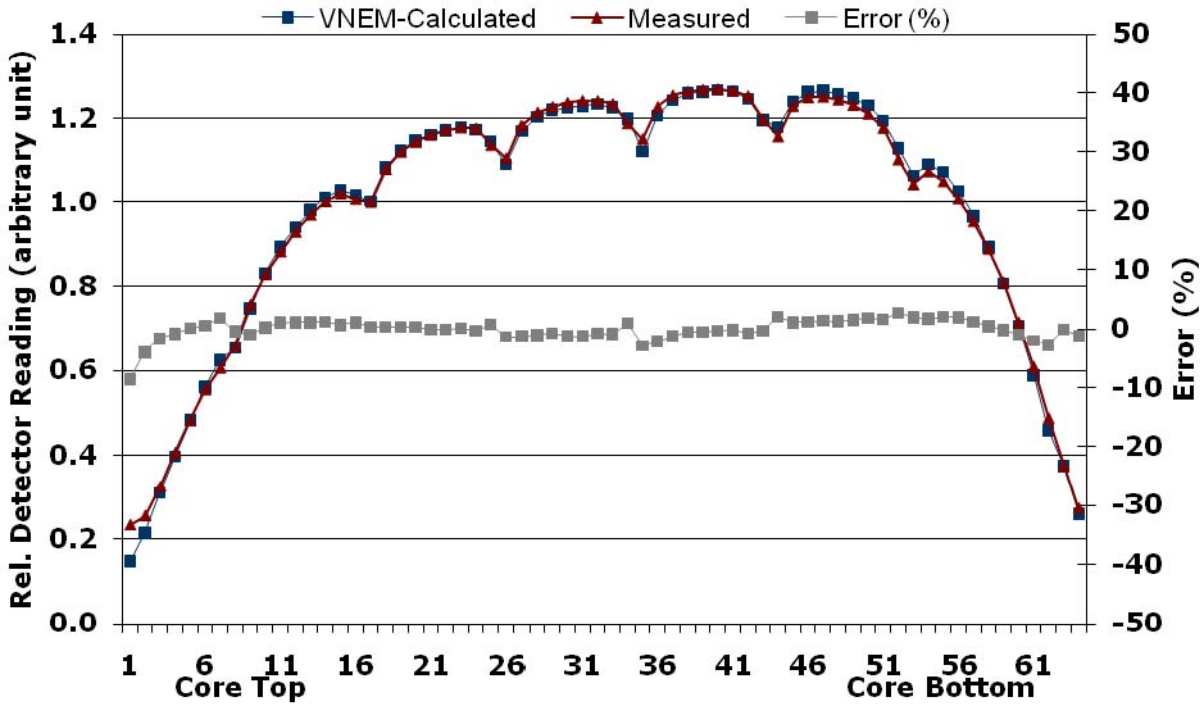

Figure 5.28: Comparison of core average axial detector readings, map 22. The readings are relative to their average.

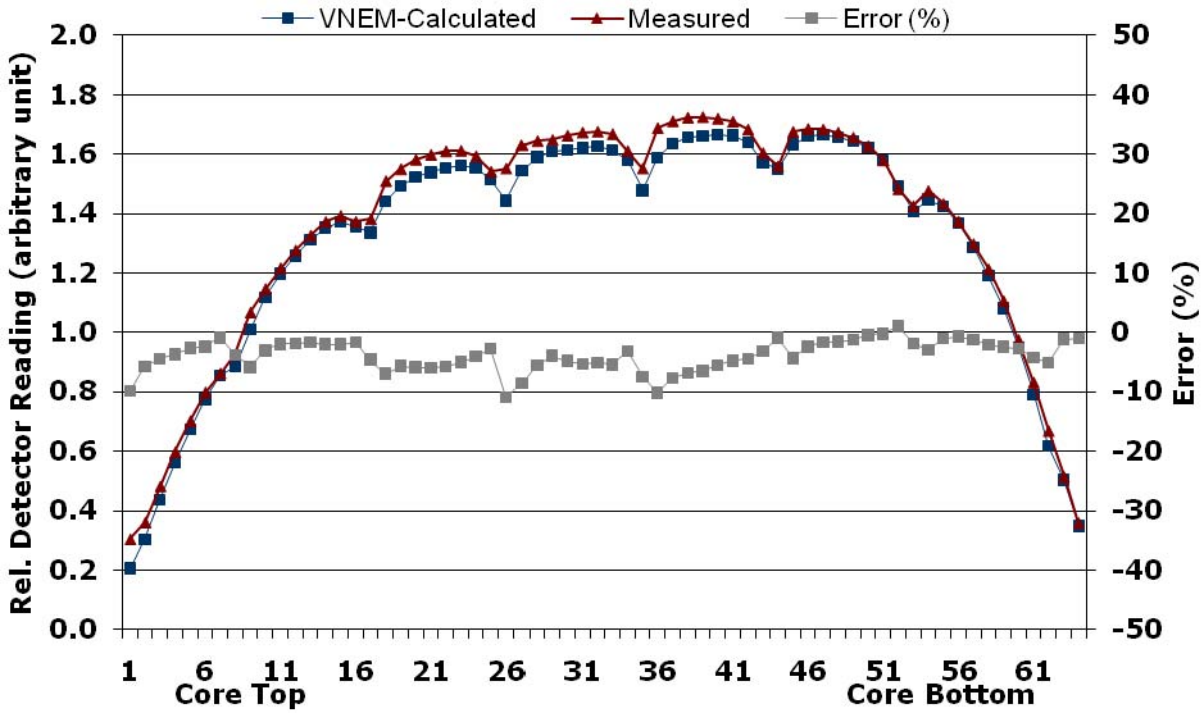

Figure 5.29: Comparison of detector readings in assembly F8, where the maximum reading is observed in map 22. The readings are relative to their average over all the measured positions in the core.

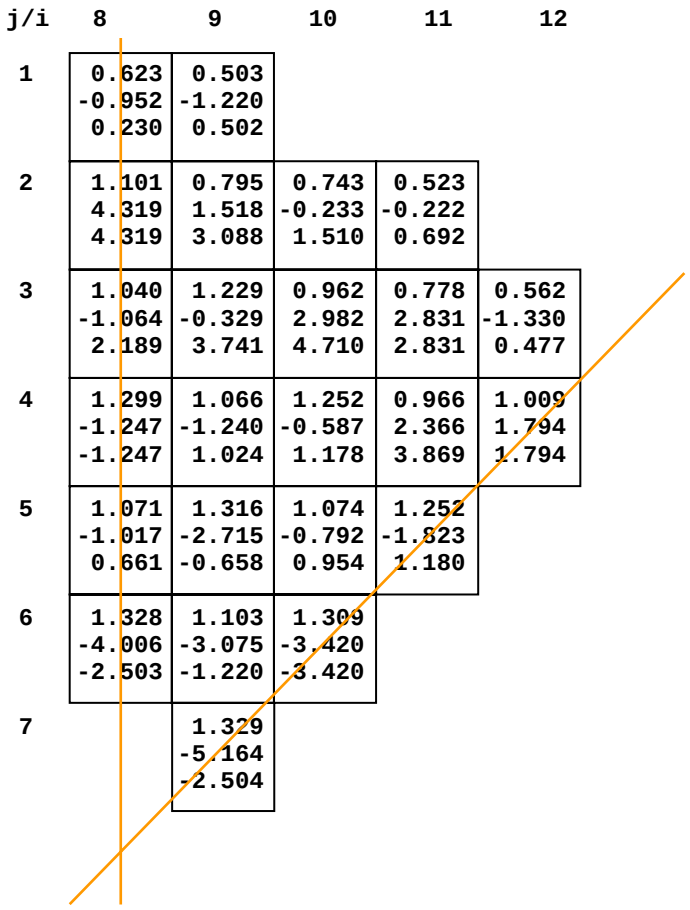

Figure 5.30: Comparison of assembly average radial detector readings, map 22. The readings are relative to their average.

Line 1: Calculated reading by CYGNUS
Line 2: CYGNUS – Upper bound of measured in %
Line 3: CYGNUS – Lower bound of measured in %

The upper and the lower bounds are taken from the maximum and the minimum readings of assemblies at octant-symmetric positions.

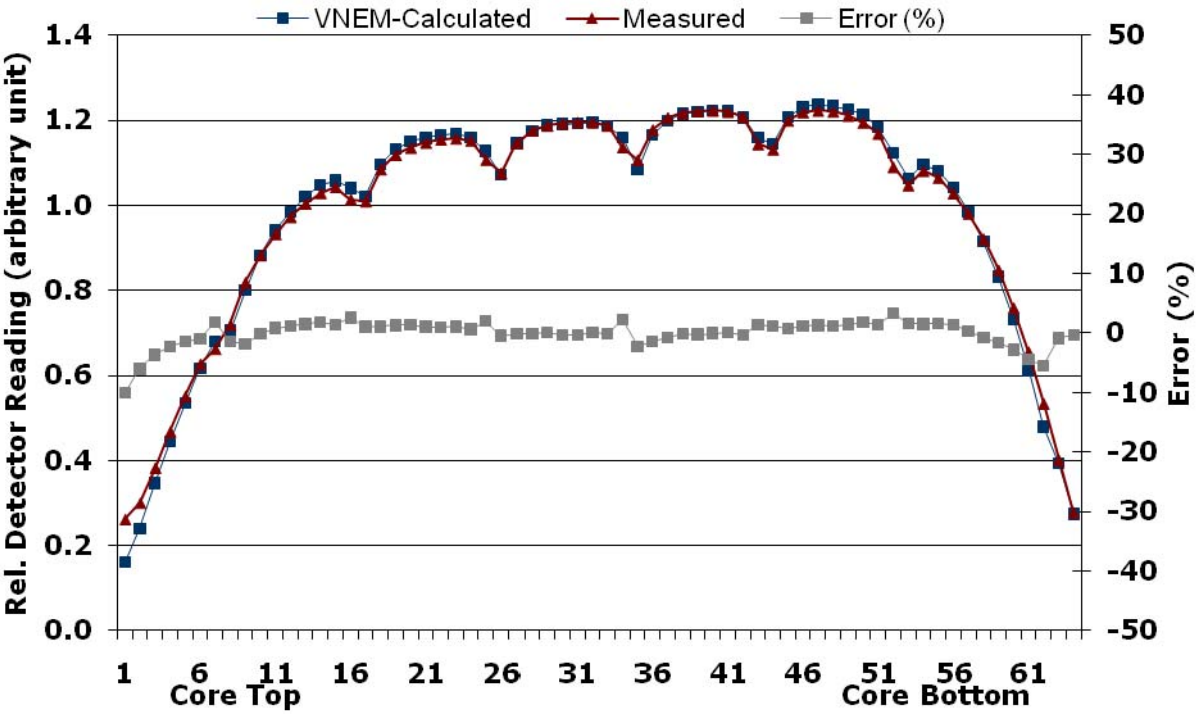

Figure 5.31: Comparison of core average axial detector readings, map 23. The readings are relative to their average.

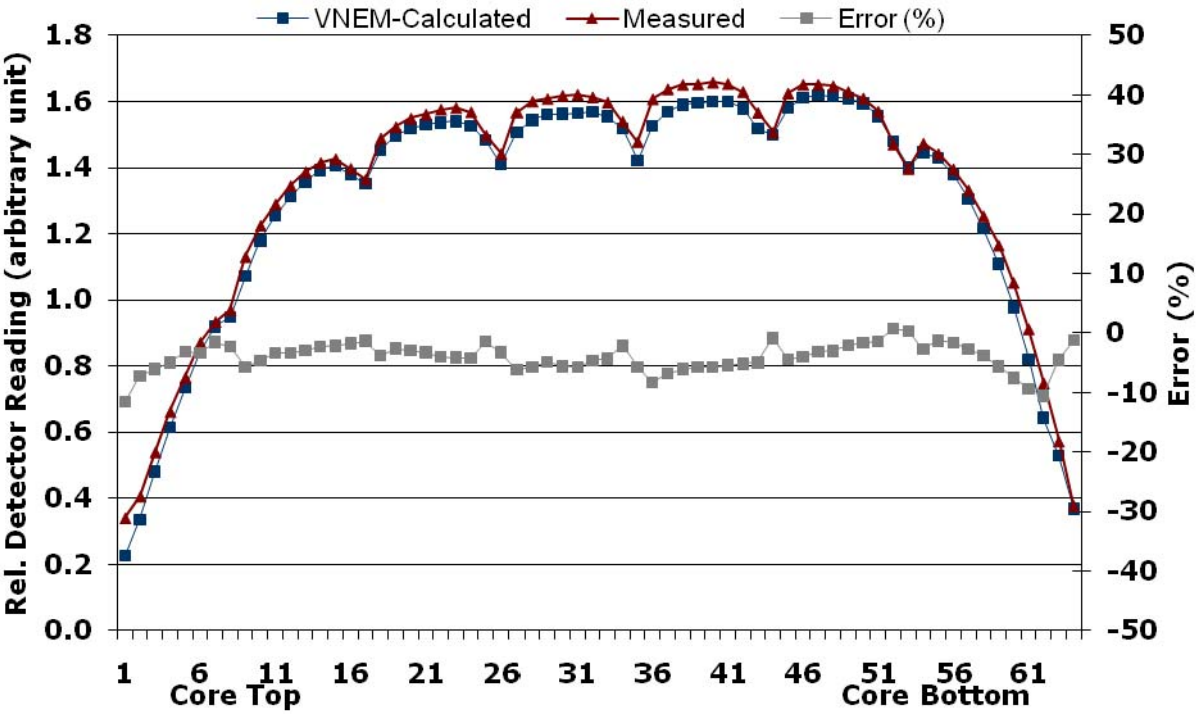

Figure 5.32: Comparison of detector readings in assembly G9, where the maximum reading is observed in map 23. The readings are relative to their average over all the measured positions in the core.

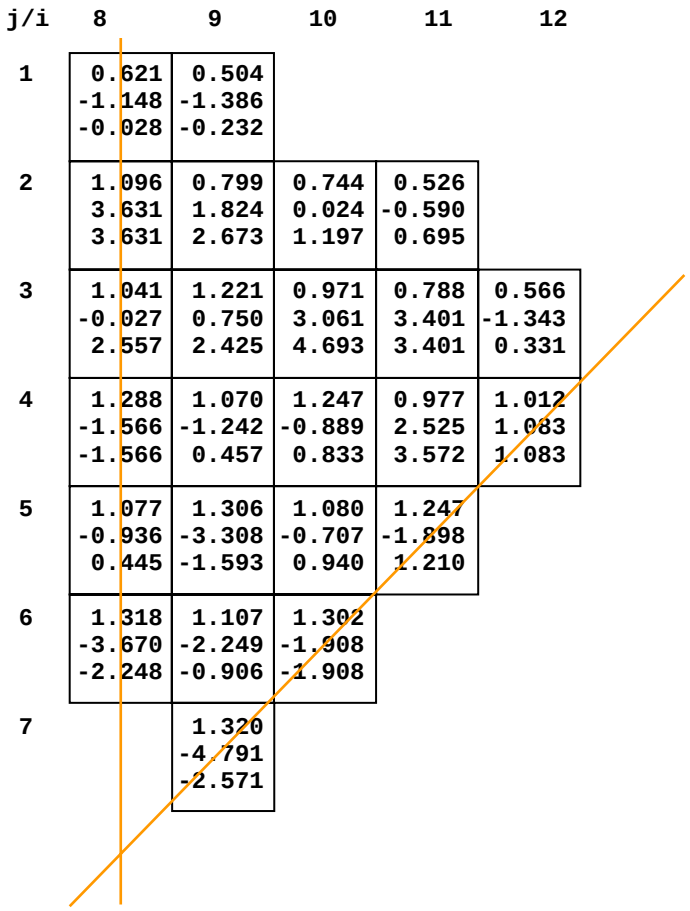

Figure 5.33: Comparison of assembly average radial detector readings, map 23. The readings are relative to their average.

Line 1: Calculated reading by CYGNUS
Line 2: CYGNUS – Upper bound of measured in %
Line 3: CYGNUS – Lower bound of measured in %

The upper and the lower bounds are taken from the maximum and the minimum readings of assemblies at octant-symmetric positions.

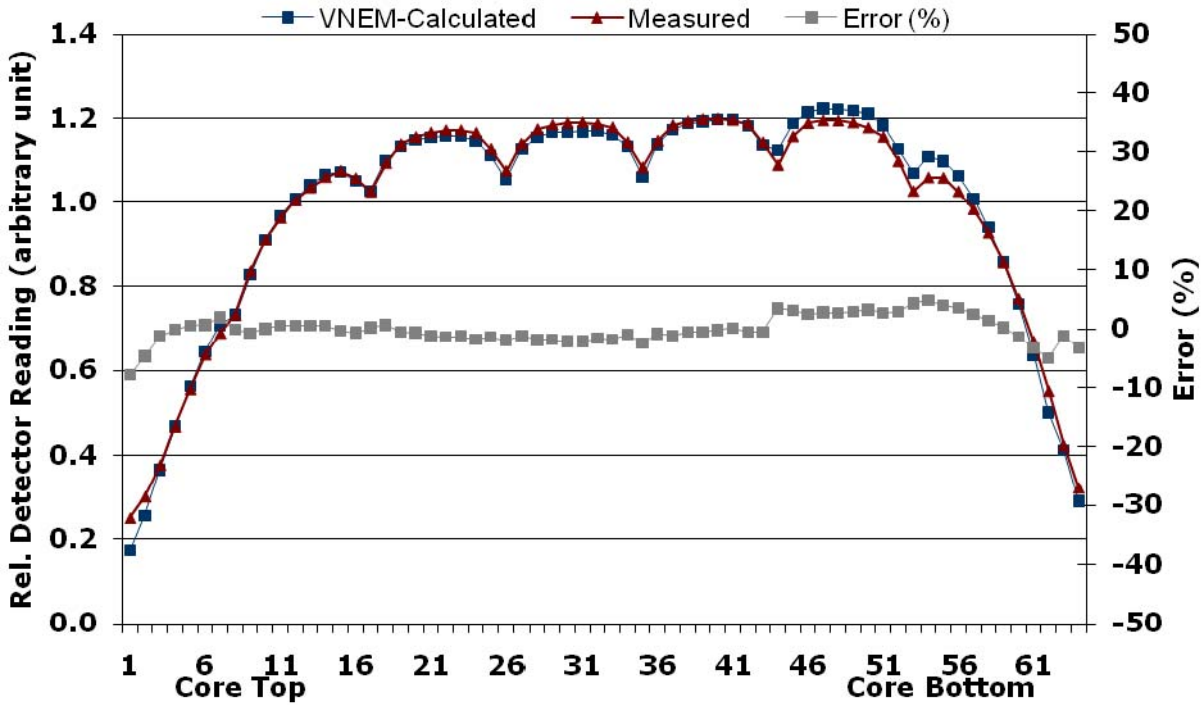

Figure 5.34: Comparison of core average axial detector readings, map 24. The readings are relative to their average.

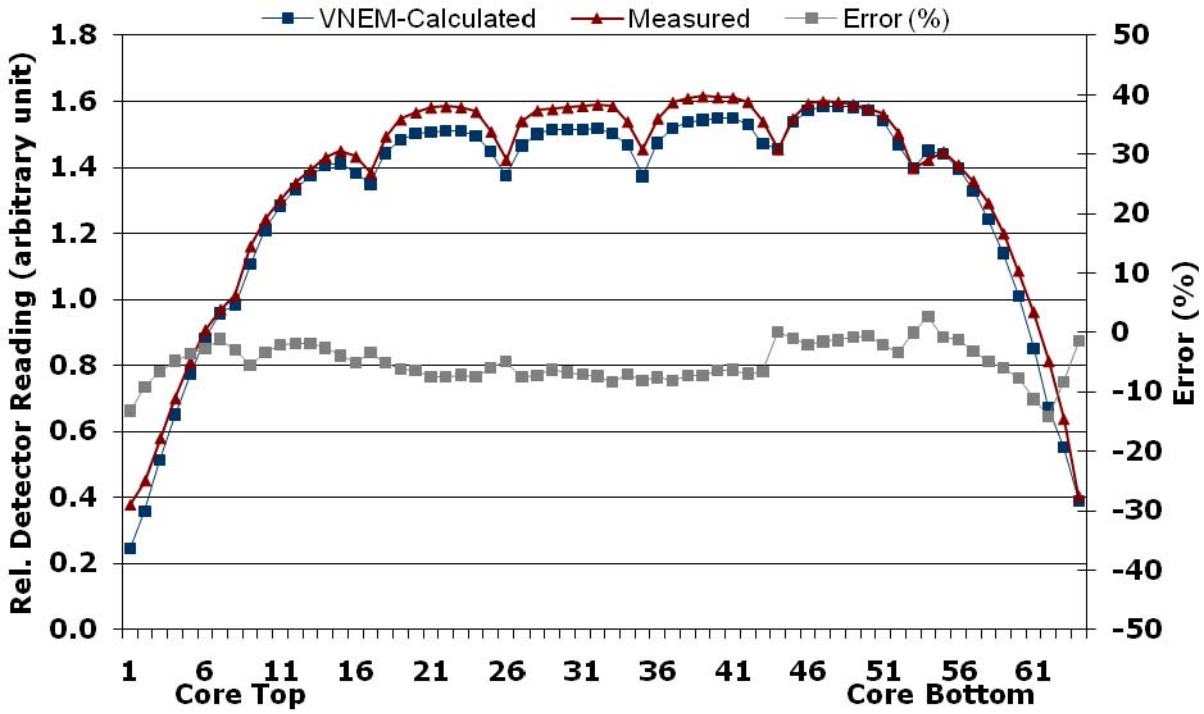

Figure 5.35: Comparison of detector readings in assembly F8, where the maximum reading is observed in map 24. The readings are relative to their average over all the measured positions in the core.

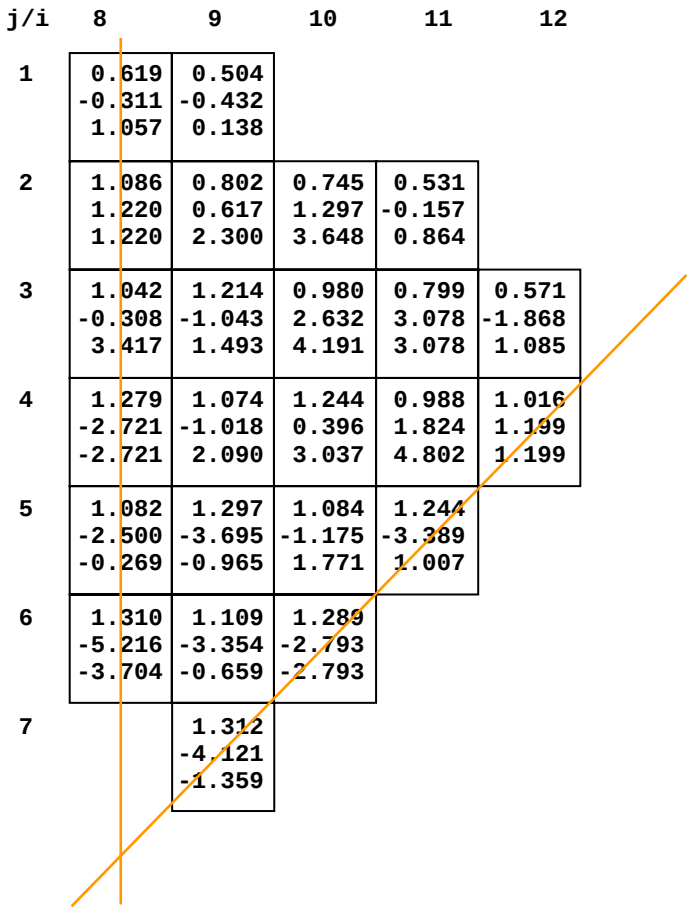

j/i	8	9	10	11	12
1	0.619 -0.311 1.057	0.504 -0.432 0.138			
2	1.086 1.220 1.220	0.802 0.617 2.300	0.745 1.297 3.648	0.531 -0.157 0.864	
3	1.042 -0.308 3.417	1.214 -1.043 1.493	0.980 2.632 4.191	0.799 3.078 3.078	0.571 -1.868 1.085
4	1.279 -2.721 -2.721	1.074 -1.018 2.090	1.244 0.396 3.037	0.988 1.824 4.802	1.016 1.199 1.199
5	1.082 -2.500 -0.269	1.297 -3.695 -0.965	1.084 -1.175 1.771	1.244 -3.389 1.007	
6	1.310 -5.216 -3.704	1.109 -3.354 -0.659	1.289 -2.793 -2.793		
7		1.312 -4.121 -1.359			

Octant symmetry lines

Figure 5.36: Comparison of assembly average radial detector readings, map 24. The readings are relative to their average.

Line 1: Calculated reading by CYGNUS
Line 2: CYGNUS – Upper bound of measured in %
Line 3: CYGNUS – Lower bound of measured in %

The upper and the lower bounds are taken from the maximum and the minimum readings of assemblies at octant-symmetric positions.

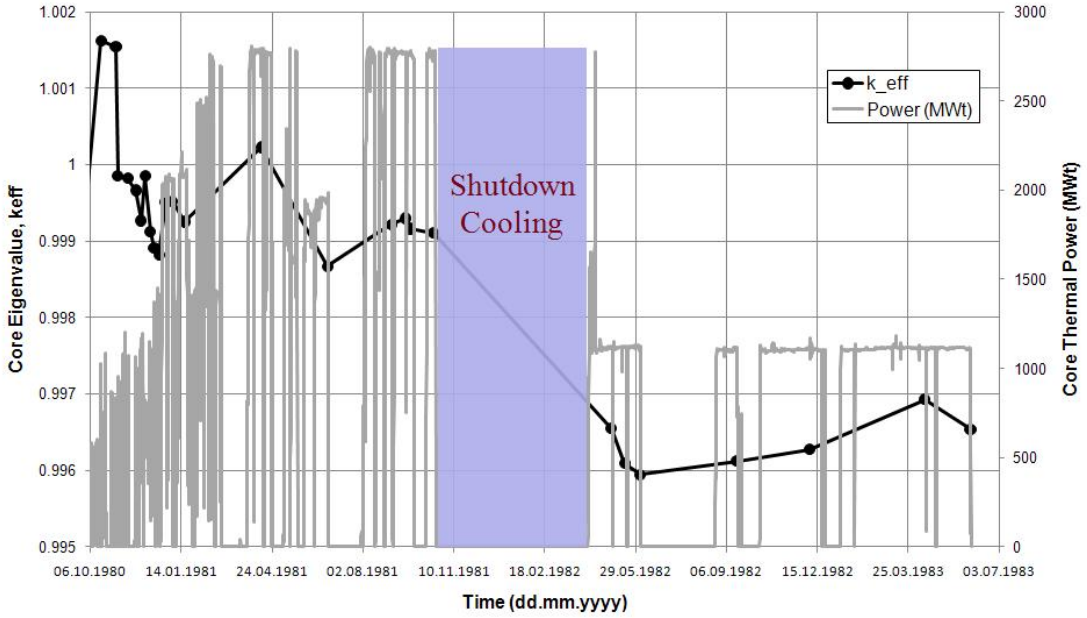

Figure 5.37: Cycle 1A shutdown cooling effect

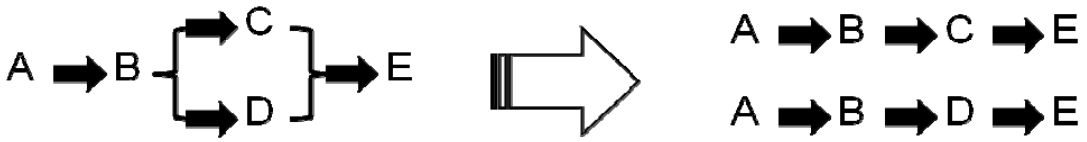

Figure 5.38: Example of the use of linearized burnup chains for isotopic tracking

5.2 Tables and Figures for Chapter 3

Table 5.2 : Typical macro cross sections of regions in 2D BWR benchmark problem

Σ^t_g: macro total cross section, fuel type 1

group	1	2	3
normal fuel rod	0.24	0.58	1.07
fuel rod with burnable poison	0.24	0.61	1.44
water rod	0.23	0.50	1.18
channel box + gap water	0.21	0.39	0.73
gap water	0.22	0.53	1.44

Σ^t_g: macro total cross section, fuel type 2

group	1	2	3
normal fuel rod	0.17	0.37	0.59
fuel rod with burnable poison	0.17	0.40	1.19
water rod	0.19	0.38	0.86
channel box + gap water	0.16	0.26	0.37
gap water	0.23	0.53	1.37

Σ^f_g: macro fission cross section, fuel type 1

group	1	2	3
normal fuel rod	0.0015	0.0040	0.044
fuel rod with burnable poison	0.0015	0.0048	0.011
water rod	0.0	0.0	0.0
channel box + gap water	0.0	0.0	0.0
gap water	0.0	0.0	0.0

Σ^f_g: macro fission cross section, fuel type 2

group	1	2	3
normal fuel rod	0.0013	0.0038	0.041
fuel rod with burnable poison	0.0013	0.0046	0.012
water rod	0.0	0.0	0.0
channel box + gap water	0.0	0.0	0.0
gap water	0.0	0.0	0.0

Table 5.2 Continued

$\Sigma_{g, g}$: macro self-scattering cross section, fuel type 1

group	1	2	3
normal fuel rod	0.20	0.50	1.00
fuel rod with burnable poison	0.20	0.52	1.00
water rod	0.17	0.42	1.17
channel box + gap water	0.19	0.35	0.72
gap water	0.16	0.43	1.43

$\Sigma_{g, g}$: macro self-scattering cross section, fuel type 2

group	1	2	3
normal fuel rod	0.15	0.33	0.53
fuel rod with burnable poison	0.15	0.34	0.76
water rod	0.15	0.32	0.86
channel box + gap water	0.16	0.24	0.37
gap water	0.17	0.43	1.36

$\Sigma_{g+1, g}$: macro scattering cross section, fuel type 1

group	1	2	3
normal fuel rod	0.033	0.053	-
fuel rod with burnable poison	0.034	0.054	-
water rod	0.056	0.083	-
channel box + gap water	0.018	0.039	-
gap water	0.061	0.101	-

$\Sigma_{g+1, g}$: macro scattering cross section, fuel type 2

group	1	2	3
normal fuel rod	0.012	0.017	-
fuel rod with burnable poison	0.012	0.017	-
water rod	0.043	0.057	-
channel box + gap water	0.0066	0.012	-
gap water	0.065	0.093	-

Table 5.3: Parameters in reference FCM2D transport calculation

method of solution	method of characteristics (MOC)
number of energy groups	3
space mesh	44 × 44 / node or assembly
polar angle mesh	20 / (0, π)
azimuthal angle mesh	80 / (0, 2π)
spacing of characteristics	≤ 0.07 cm

Table 5.4: Parameters in VNEM3D transport calculation

PL order		5
source expansion order [2.3]	nr = 1	$P_0(x)$, $P_0(y)$
	nr = 2	$P_1(x)$, $P_0(y)$
	nr = 3	$P_0(x)$, $P_1(y)$
	nr = 4	$P_1(x)$, $P_1(y)$
	nr = 5	$P_2(x)$, $P_0(y)$
	nr = 6	$P_0(x)$, $P_2(y)$
	nr = 7	$P_4(x)$, $P_0(y)$
	nr = 8	$P_0(x)$, $P_4(y)$
boundary value expansion order [2.3]	sr = 1	$P_0(x)$
	sr = 2	$P_1(x)$
	sr = 3	$P_2(x)$

Table 5.5: Core eigenvalue comparison of 2D BWR benchmark problem

Case	keff(FCM2D, reference)	keff(VNEM3D)	error in %
1	1.044472	1.043557	–0.09
2	0.893869	0.893990	0.01

Table 5.6: Relative nodal power comparison of 2D BWR benchmark problem

Case 1

1.081 1.079 –0.2	1.114 1.125 1.1
0.725 0.716 –0.9	1.081 1.079 –0.2

Case 2

1.107 1.114 0.7	0.842 0.845 0.3
0.945 0.928 –1.7	1.107 1.114 0.7

line 1: relative nodal power by FCM2D (reference)
line 2: VNEM3D
line 3: error in %

Table 5.7: Relative nodal maximum cell power comparison of 2D BWR benchmark problem

Case 1

1.085 1.085 0.0	1.089 1.098 0.9
0.742 0.732 –1.0	1.085 1.085 0.0

Case 2

1.105 1.101 –0.4	0.930 0.918 –1.2
0.860 0.881 2.1	1.105 1.101 –0.4

line 1: relative nodal maximum cell power by FCM2D (reference)
line 2: VNEM3D
line 3: error in %

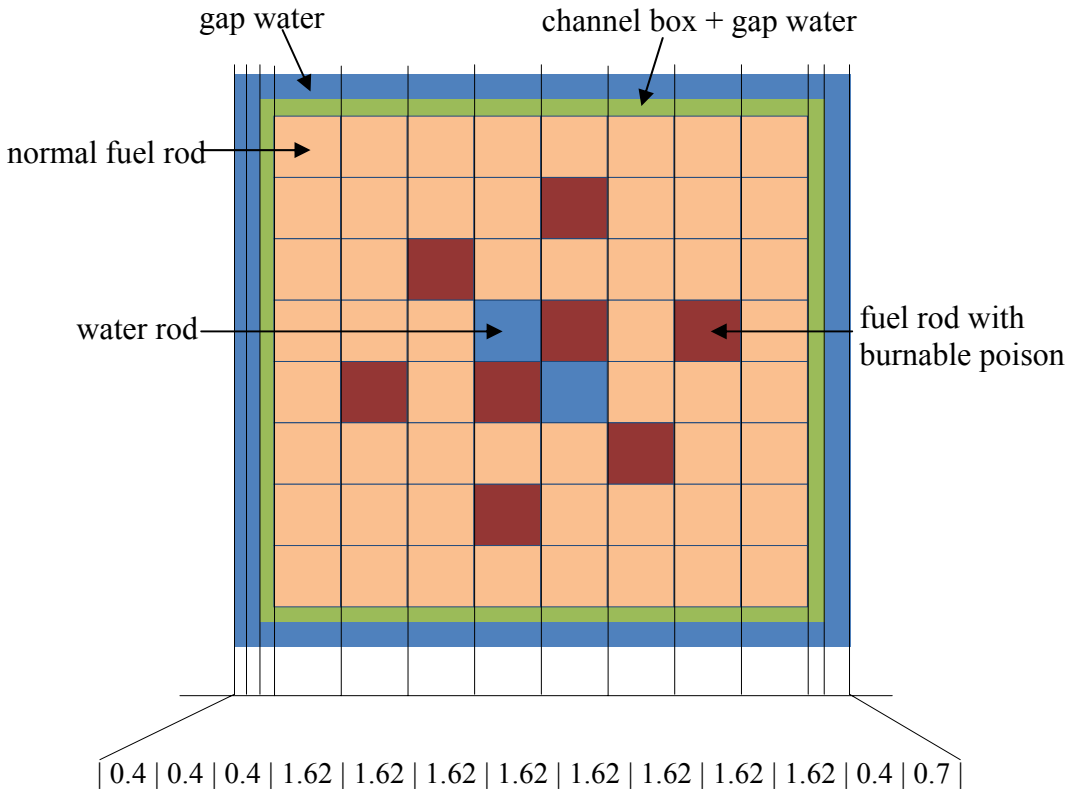

Figure 5.39 : Geometry of assemblies in 2D BWR benchmark problem

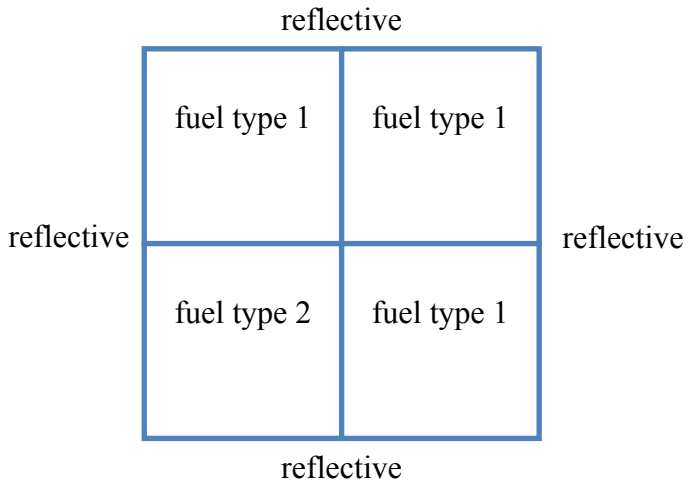

(1) Case 1

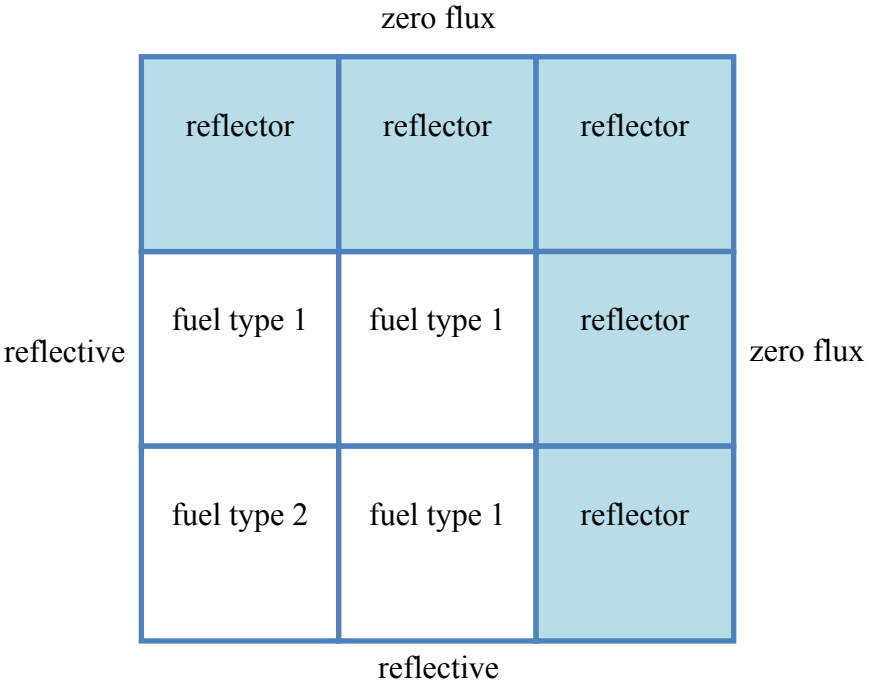

(2) Case 2

Figure 5.40: Assembly configuration of 2D BWR benchmark problem

Bibliographic Data Sheet **NKS-231**

Title	Comparison of VNEM to Measured Data from Ringhals Unit 3 (Phase 3)
Author(s)	Makoto Tsuiki and Steven Mullet
Affiliation(s)	Institutt for energiteknikk, OECD Halden Reactor Project, Norway
ISBN	978-87-7893-302-7
Date	January 2011
Project	NKS-R / IACIP, NKS-R-2008-61
No. of pages	44
No. of tables	7
No. of illustrations	39
No. of references	7

Abstract

1. PWR
Comparisons have been made of a PWR core simulator CYGNUS with VNEM neutronics module to the measured data obtained from Ringhals unit 3 NPP through the cycle 1A (core average burnup = 0 through 10,507MWD/MT).
The results can be summarized as:
core eigenvalue = 0.99937 +/- 0.00086 before intermediate
5 months shutdown
core eigenvalue = 0.99647 +/- 0.00029 after intermediate
5 months shutdown
The reason of core eigenvalue drop after the intermediate shutdown is estimated to be the build-up of fissile elements during the long shutdown. A calculation model to track some important isotopes in addition to Xe135 and Sm149 (these isotopes are tracked in the present version of CYGNUS) has to be implemented.
As for the comparison of the neutron detector readings, the agreement was excellent throughout the cycle 1A as observed in Phase 1 and 2 (2008, 2009).
The burnup tilt effect was not observed during the cycle 1A. The verification of the burnup tilt model of CYGNUS will be performed in the next phase of the project.
2. BWR
A preliminary 2D numerical benchmarking was performed for BWR cores. The problems were generated imitating the NEACRP MOX PWR 2D benchmark problems. The results of comparisons of VNEM to a reference transport code (FCM2D), based on the method of characteristics, were as good as those obtained in the case of PWR cores for similar benchmarking.

Key words CYGNUS, VNEM, Ringhals, unit 3, PWR, neutron detector, keff, BWR, benchmark,
IACIP: NKS_R_2008_61

Available on request from the NKS Secretariat, P.O.Box 49, DK-4000 Roskilde, Denmark.
Phone (+45) 4677 4045, fax (+45) 4677 4046, e-mail nks@nks.org, www.nks.org